# DILATATION, FLAME STRAIN, DISPLACEMENT SPEED AND CURVATURE IN TURBULENT PREMIXED FLAMES USING DIRECT NUMERICAL SIMULATION

# DILATATION, FLAME STRAIN, DISPLACEMENT SPEED AND CURVATURE IN TURBULENT PREMIXED FLAMES USING DIRECT NUMERICAL SIMULATION

By

NASIM SHAHBAZIAN, M.Sc.

A Thesis

Submitted to the School of Graduate Studies

in Partial Fulfillment of the Requirements

for the Degree

Master of Applied Science

McMaster University

MASTER OF APPLIED SCIENCE (2008)
(Mechanical Engineering)

McMaster University
Hamilton, Ontario

TITLE: Dilatation, Flame Strain, Displacement Speed and Curvature in Turbulent Premixed Flames Using Direct Numerical Simulation

AUTHOR: Nasim Shahbazian, M.Sc. (Chalmers University of Technology)

SUPERVISOR: Dr S. Tullis, Ph.D.

NUMBER OF PAGES: xv, 83.

*To Jonathan Gustafsson*

# Abstract

The relationship between dilatation, displacement speed, flame tangential strain rate and flame normal velocity gradient for a premixed turbulent flame in a corrugated/wrinkled flame regime is analyzed. The decomposition of dilatation into the flame tangential and normal strains and their relationship with curvature is studied.

Three-dimensional, fully compressible direct numerical simulations (DNS) of premixed flames in a cube have been performed using a uniform $256^3$ grid. For the turbulent case, decaying isotropic homogeneous turbulent velocity field is considered with an initial turbulence spectrum imposed. Simple single-step chemistry with an Arrhenius reaction rate is used. This simplification is valid as the flame considered is in the corrugated/wrinkled regime where the flame thickness is smaller than the smallest scales of turbulence. A single laminar flame is initially inserted into the turbulent field.

A strongly linear relationship between dilatation and curvature has been seen which is due to the high correlation of displacement speed with curvature. The correlation between tangential strain rate and curvature is shown to be negative with a breakdown due to the curvature reaching the scale of the flame thickness at the cusps. To isolate the effect of heat release and turbulence, cases of a laminar sinusoidal wrinkled flame and a turbulent $\tau$=0 flame have been carried out. For a laminar sinusoidal wrinkled flame, a negative correlation between $a_t$ and curvature was seen. This contradicts previous hypotheses (Haworth and Poinsot, 1992) (Chakraborty and Cant, 2004) where the negative correlation between $a_t$ and curvature was explained to be due to different turbulence levels in front and behind the flame. Turbulence and alignment of flame surface with expansive tangential strains is shown to be responsible for the scatter seen in $a_n$ and $a_t$ relationships with curvature. Changing the peak reaction location towards the front of the flame did not change the trend in the plots of dilatation, tangential and normal strain rates versus curvature, confirming that dilatation relationship with curvature in particular is not due to any curvature distortion of the flame interior. However, it did

thicken the flame and reduce the dilatation (and consequently its components, $a_n$ and $a_t$) plot versus curvature and the magnitude of their curvature dependence.

# Acknowledgements

I would like to thank Dr. Tullis for the great supervision and mentoring. I would also like to thank Catherine Strutt and James Strack for their help and suggestions. The financial support of NSERC and the computational facilities of SHARCNET are also gratefully acknowledged. Finally, I give my appreciation to the faculty and staff of department of Mechanical Engineering for their support and insightful help.

# Contents

# List of Figures

# List of Tables

# Nomenclature

***English Characters***

| | |
|---|---|
| $a_0$ | acoustic speed |
| $a_n$ | normal strain rate |
| $a_t$ | tangential strain rate |
| $B$ | pre-exponential factor |
| $c$ | reaction progress variable |
| $C_V$ | specific heat at constant volume |
| $C_P$ | specific heat at constant pressure |
| $D$ | molecular diffusivity |
| $E$ | internal energy |
| $E_a$ | activation energy |
| $F$ | flame cross sectional area |
| $h$ | enthalpy of formation |
| $H$ | heat of the reaction per unit mass of mixture |
| $Ka$ | Karlovitz number |
| $Ka_\delta$ | Karlovitz number for the inner layer thickness |
| $l$ | integral length scale |
| $L_{BOX}$ | computational domain size |
| Le | Lewis number |
| $m$ | mass |
| $\dot{m}$ | mass flux |
| $Ma$ | Mach number |
| $n$ | direction normal to the flame |
| $N$ | local flame normal vector |
| $N$ | number of data points |
| $P$ | pressure |
| Pr | Prandtl number |
| $q$ | heat flux |
| Re | Reynolds number |
| $R$ | specific gas constant |
| $R_{ij}$ | two-point correlation |
| $R^0$ | universal gas constant |
| Sc | Schmidt number |
| $S_d$ | flame displacement speed |
| $S_L$ | laminar flame speed |
| $S_T$ | turbulent flame speed |

| | |
|---|---|
| $S_u$ | skewness factor of the velocity derivatives |
| $t$ | time |
| $t$ | direction tangential to the flame |
| $t_l$ | integral time scale |
| $t_k$ | Kolmogorov time scale |
| $t_{chem}$ | chemical time scale |
| $T$ | temperature |
| $\hat{T}$ | instantaneous dimensional temperature |
| $T_{ad}$ | adiabatic flame temperature |
| $u$ | instantaneous velocity |
| U | mean velocity in *x*-direction |
| V | mean velocity in *y*-direction |
| W | mean velocity in *z*-direction |
| $V$ | diffusion velocity |
| $x$ | distance |

***Greek Characters***

| | |
|---|---|
| $\alpha$ | heat released by the flame |
| $\beta$ | Zeldovich number |
| $\nu$ | kinematic viscosity |
| $\rho$ | density |
| $\tau$ | heat release factor |
| $\tau_{ij}$ | viscous stress |
| $\kappa$ | wavenumber |
| $\mu$ | dynamic viscosity |
| $\lambda$ | thermal conductivity |
| $\kappa_m$ | mean curvature of the flame |
| $\gamma$ | ratio of specific heats |
| $\gamma_E$ | initial kinetic energy constant |
| $\eta$ | Kolmogorov length scale |
| $\dot{\omega}$ | reaction rate |
| $\delta_L$ | laminar flame thickness |
| $\delta_R$ | reaction zone thickness |
| $\Delta t$ | time step |
| $\Delta x$ | grid spacing |
| $\nabla \cdot u$ | dilatation |

***Overbars***

$\overline{(\ )}$ time averaged value

***Subscripts***

| | |
|---|---|
| $(\ )_i$ | the $i^{th}$ direction |
| $(\ )_j$ | the $j^{th}$ direction |
| $(\ )_k$ | the $k^{th}$ direction |
| $(\ )_\alpha$ | property of the $\alpha^{th}$ specie |
| $(\ )_F$ | property of the fuel |
| $(\ )_P$ | property of the products |
| $(\ )_R$ | property of the reactants |
| $(\ )_0$ | property of the reactants (reference) |
| $(\ )_L$ | property of laminar flow |
| $(\ )_t$ | property of turbulent flow |

***Superscripts***

$(\ )'$ fluctuating component

***Acronyms***

| | |
|---|---|
| 2D | two-dimensional |
| 3D | three-dimensional |
| CFL | Courant-Friedrichs-Levy |
| DNS | direct numerical simulations |
| FSD | flame surface density |
| LES | large eddy simulations |
| MPI | message passing interface |
| NSCBC | Navier-Stokes characteristic boundary condition |
| PDF | probability density function |
| RANS | Reynolds-averaged Navier-Stokes |
| SDF | surface density function |
| SGS | sub-grid scale |

# Chapter 1

# Introduction

### *1.1 Background*

Combustion systems are divided into premixed and non-premixed configurations. In premixed combustion, fuel and oxidizer are mixed before entering the combustion chamber while in non-premixed combustion; they enter separately. Premixed flames are widely used for industrial applications; some examples include Bunsen burners, stationary gas turbines and spark ignition engines. The study and understanding of these flames is an important issue in order to develop and improve combustion systems. The necessity of pollution control, increasing efficiency and decreasing fuel consumption in combustion engines highlights the importance of premixed flame studies. In most practical combustion systems, premixed flames are in turbulent environments. The structure of premixed flames in turbulent flows is a very important and fundamental issue in the field of combustion. Due to difficulties of studying flame structure experimentally, numerical simulations have become a powerful tool for understanding the complex interaction between combustion and turbulence. Recent improvements in computer size and speed have made it possible to use direct numerical simulations (DNS). In DNS, the Navier-Stokes equations are numerically solved without any turbulence modeling. This means that the whole range of spatial and temporal scales of the turbulence must be resolved. The information obtained by DNS can be used for model development and testing for Reynolds averaged Navier-Stokes (RANS), large eddy simulations (LES), and fundamental understanding of the flame behaviour.

Combustion is a very complicated phenomenon since it contains a large range of chemical time and length scales. Performing DNS is computationally demanding for turbulent premixed flames and it has been mainly limited to simple finite-rate chemistry, low Reynolds numbers and very simple geometries. Most recent turbulent premixed flame simulations have been carried out either in two dimensions using complex chemistry, or in three dimensions with simplified chemistry. The latter approach is used for the present study.

Flame wrinkling is one of the most important mechanisms controlling turbulent flame behaviour. A flame front propagating in a non-uniform flow is subject to strain which leads to changes in flame curvature, flame area, burning velocity, fuel consumption and other properties. Many of these changes also in turn affect each other, so flame curvature, strain, dilatation (the gas expansion, $\nabla \cdot \boldsymbol{u}$, due to the heat release in the flame) and velocity gradient have a significant effect on structure, propagation, and extinction of turbulent flames. Understanding these effects and relations can be really useful in flow modeling as well as design purposes.

The gas dilatation is the sum of the flame tangential and normal strains and consideration of this relationship is helpful in understanding of flame strain behaviour. In particular, investigating the flame normal strain rate (or flame normal velocity gradient) is useful, since this term is important in scalar transport, and especially counter-gradient transport in flames. Normal and tangential strain rates influence the scalar flux and reaction rate modeling for both RANS and LES. Dilatation and the flame strains are also important for flame surface density (FSD) treatments in RANS and LES modeling.

Most previous work on premixed flame strain has focused on flame tangential strains, their relationship with flame curvature and their effect on flame speeds. As a propagating surface, the alignment of the flame with the turbulent fluid strains depends on the ratio of local (laminar) flame speed to strain rate. The flame also wrinkles inherently as a thin propagating surface and due to instabilities such as Darrius-Landau (Law and Sung, 2000). Heat release (and the dilatation of the gas across such curved surfaces) then produces flame tangential strains. There are limited studies focused on the effect of dilatation on the flame and the dilatation dependence on flame curvature, flame strains and displacement speed.

## *1.2 Objective and Scope*

In this work, the interdependence of dilatation, tangential and normal strain rates, flame displacement speed and curvature in turbulent premixed flames are studied using direct numerical simulations in three-dimensional configuration. Simplified chemistry is assumed and the influence of turbulence, heat release and reaction rate profile are isolated by performing different DNS cases.

## *1.3 Outline of the Thesis*

This thesis is divided into five chapters. Chapters one and two include the introduction, background and literature review on DNS of turbulent premixed flames and flame properties such as strain, dilatation and displacement speed. In the background section, the properties of turbulent premixed flames and the regimes for turbulent combustion are explained. The previous direct numerical simulations studies on turbulent premixed flames are reviewed and discussed with focus on the studies on flame curvature, strains, dilatation and displacement speed.

The numerical details of the DNS code used are explained in chapter 3. The governing equations and assumptions are detailed and explained. The section continues with details of boundary conditions and numerical schemes used for the simulations. Four different cases are considered, and the numerical details and properties used for each of these cases are explained. A preliminary analysis for validation and testing of the code is shown in the appendix.

The four cases of premixed flames which are examined in this study are: a turbulent flame, a laminar sinusoidal flame, a turbulent cold flame and a laminar sinusoidal flame where reaction rate peak is shifted towards the front of the flame. The results are shown in chapter 4 and cases are compared and analyzed in depth. The work is concluded with a summary of the results in chapter 5 and some recommendations for future work.

# Chapter 2

# Background and Literature Review

Combustion can be simply defined as following:

Fuel + Oxidizer → Products + Heat

and can be divided into premixed and non-premixed combustion. In premixed combustion, fuel and oxidizer are mixed before entering the combustor and a flame propagates through the mixture, while in the non-premixed combustion fuel and air enter the combustion chamber separately and react where they meet.

Turbulent premixed combustion corresponds to the propagation of a flame in a turbulent reactant flow. The turbulence can convect and distort the flame, and this, in turn, can affect the flame behaviour. Here, a background and critical literature review of premixed flames, their interaction with turbulence and the relevant numerical techniques are presented.

## *2.1 Computational Approaches for Turbulent Combustion*

Different computational approaches for turbulent combustion are used as follows:

Reynolds-Averaged Navier-Stokes (RANS) method involves time averaging of the governing equations and solving the equations for the mean values of all quantities. The effects of all of the scales of turbulence must be modeled. The RANS method is computationally cheap, models for isothermal flows are (fairly) well developed (much less so for reacting flows) and commercial codes are available.

In Large Eddy Simulations (LES) the equations are filtered (volume averaged), so the large turbulent scales are calculated whereas the effects of small turbulent scales on combustion are considered by using sub-grid scale models. This method is intermediate in expense. Models for reacting flows are still being developed.

Direct Numerical Simulation (DNS) is another method of solving a flow field computationally. Here, all of the scales of the turbulence are calculated, so it is computationally very expensive. Since this method is used in the present work, it will be explained in more details in the following section.

## *2.2 Direct Numerical Simulations*

Turbulence is a solution to the Navier-Stokes equations for high Reynolds number flows. It is a state of the flow characterized by chaotic and random three-dimensional vorticity and is irregular, diffusive, and dissipative. Turbulent flow consists of velocity fluctuations with a range of time and length scales. In a turbulent flow, kinetic energy is extracted from the mean flow mainly by the largest of these scales to smaller and smaller scales down to the Kolmogorov scales (Kolmogorov, 1941) where the kinetic energy is transferred to internal energy.

In Direct Numerical Simulations (DNS), the Navier-Stokes equations are solved numerically by resolving all of the turbulent scales. Consequently, the full instantaneous Navier-Stokes equations are solved and there is no modeling involved. All flow quantities and their gradients can be obtained directly from the simulations. However, this method requires extremely large computer resources and can only be carried out for low Reynolds numbers and simplified geometries. High order numerical schemes are also required to ensure that numerical effects (e.g. numerical diffusion) do not affect the solution. The first DNS of decaying homogenous isotropic turbulence was performed by Orszag and Patterson (1972) on $32^3$ grids. Since then, DNS has become a powerful tool for understanding of turbulent flows and model development.

### *2.3 Premixed Flames*

Combustion involves multiple reactions and multiple species. The mass fraction $Y_\alpha$ for any species is defined by:

$$Y_\alpha = \frac{m_\alpha}{m} \tag{2.1}$$

where $m_\alpha$ is the mass of each species and $m$ is the total mass.

A reaction progress variable can be defined as:

$$c = \frac{Y_P - Y_{P_0}}{Y_{P_\infty} - Y_{P_0}} \tag{2.2}$$

where $Y_P$ is the mass fraction of the product species and it goes from 0 in the fresh gases to 1 in the products. Indices 0 and $\infty$ represent reactants and products respectively.

The transport equation for reaction progress variable, $c$, is given by:

$$\frac{\partial(\rho c)}{\partial t} + \frac{\partial(\rho u_k c)}{\partial x_k} = \frac{\partial}{\partial x_k}\left[\rho D \frac{\partial c}{\partial x_k}\right] + \dot{\omega} \tag{2.3}$$

where $D$ is diffusion coefficient and $\dot{\omega}$ is the chemical source term. $\rho$ is density and $u_k(\vec{x},t)$ represents the $k$-th component of the fluid velocity at a point in space $\vec{x}$ and time, $t$.

A simple relation used for determining the laminar flame speed ($S_L$) is based on the consumption of reactants as:

$$S_L = -\frac{1}{\rho_0 Y_F^0}\int_{-\infty}^{+\infty} \dot{\omega}_F dx \tag{2.4}$$

where $\dot{\omega}_F$ is the fuel reaction rate which is negative. Since in this work one-step simple chemistry is assumed and the reactant consists of one species and reactant density is set as 1, the relation for laminar flame speed is just:

$$S_L = \int_{-\infty}^{+\infty} \dot{\omega} dx \tag{2.5}$$

The laminar flame thickness may be defined in two different ways. It can be expressed as the distance over which reaction progress variable ($c$) changes over a specified $c$ range (typically from $c$=0.01 to $c$=0.99). In figure 2.1 this thickness is shown by $\delta_L^t$. A more useful expression for the laminar flame thickness is obtained by using the reaction progress variable profile and computing:

$$\delta_L = \frac{1}{\max\left(\left|\frac{\partial c}{\partial x}\right|\right)} \tag{2.6}$$

which is also shown in figure 2.1.

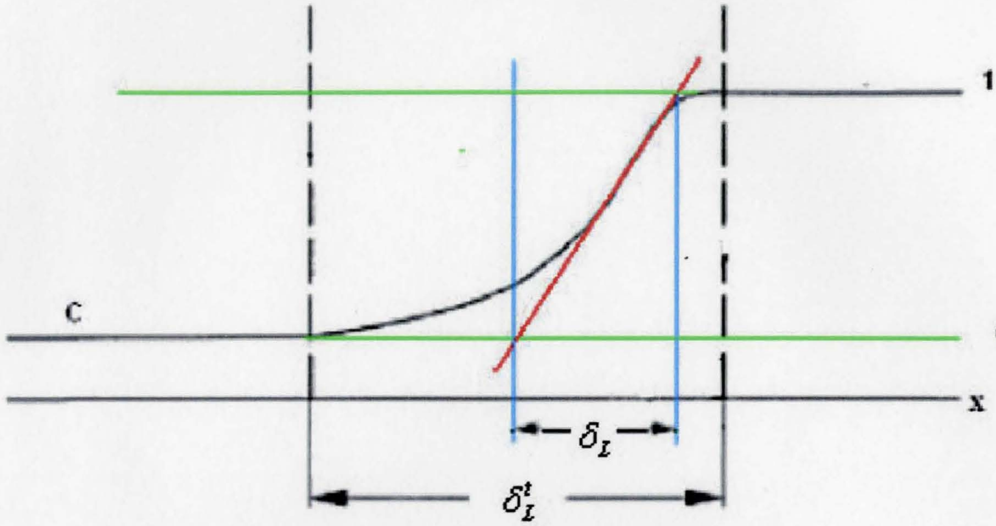


Figure 2.1: Definitions of flame thickness for a premixed flame.

For a single isosurface at $c=c^*$, the reaction progress variable equation (equation 2.3) can be written as: (Poinsot and Veynante, 2005)

$$\left[\frac{\partial c}{\partial t}+u_k\frac{\partial c}{\partial x_k}\right]_{c=c^*}=S_d\left|\nabla c\right|_{c=c^*} \tag{2.7}$$

where $S_d$ is the displacement speed at $c=c^*$.

By using the continuity and the reaction progress variable equations, $S_d$ on a single isosurface can be written as: (Echekki and Chen, 1996)

$$S_d=\frac{\dot{\omega}\big|_{c=c^*}+\dfrac{\partial}{\partial x_k}\left[\rho D\dfrac{\partial c}{\partial x_k}\right]_{c=c^*}}{\rho_{c=c^*}\sqrt{\dfrac{\partial c}{\partial x_k}\dfrac{\partial c}{\partial x_k}}\big|_{c=c^*}} \tag{2.8}$$

The flame tangential strain rate $a_t$, the flame normal velocity gradient, $a_n$, the dilatation, $\nabla\cdot u$ and curvature are defined as:

$$a_t = \left(\delta_{ij} - N_i N_j\right)\frac{\partial u_i}{\partial x_j}\Big|_{c=c^*} \tag{2.9}$$

$$a_n = \frac{\partial u_n}{\partial n}\Big|_{c=c^*} \tag{2.10}$$

$$\nabla \cdot u = a_t + a_n = \frac{\partial u_k}{\partial x_k}\Big|_{c=c^*} \tag{2.11}$$

$$\kappa_m = \frac{\partial N_k}{\partial x_k}\Big|_{c=c^*} \tag{2.12}$$

where $n$ and $t$ signify the directions normal and tangential to the flame respectively and $N_i$ is the $i$-th component of the local flame normal vector. Positive curvature is convex towards the reactants. The dilatation, flame displacement speed, flame tangential and normal strain rates are affected by the flame curvature and indicate the flame behaviour. Both turbulence and heat release can provide tangential and normal strains. The study of these properties and their dependence on curvature is necessary in understanding of premixed flames and is useful for the development of models for RANS and LES.

Dilatation is a measure of the excess volume created by the heat release through the flame. It is controlled by the reaction rate and diffusion on the right hand side of the progress variable equation and can be expressed in terms of displacement speed, gradient of progress variable and heat release factor, $\tau = \frac{\rho_R}{\rho_P} - 1$ (Chakraborty and Cant, 2004)

$$\frac{\partial u_k}{\partial x_k}\Big|_{c=c^*} = \frac{\tau S_d |\nabla c|}{(1 + \tau c)}\Big|_{c=c^*} \tag{2.13}$$

A linear relationship between displacement speed $S_d$ and curvature has been noted by Echekki and Chen (1996, 1999), and it is a key determinant of the correlation between dilatation and curvature.

### 2.4 Turbulent Flames

Turbulence stretches and wrinkles the laminar flames, consequently increasing the flame surface area, burning more reactant and causing a higher combustion rate and turbulent flame speed.

Damköhler (1940) was the first person who presented an equation for a turbulent flame speed. He related the mass flux of reactant, $\dot{m}$ to the flame surface area which is produced by turbulence, $F_T$ and laminar flame speed, $S_L$ as follows:

$$\dot{m} = \rho_0 S_L F_T = \rho_0 S_T F \tag{2.14}$$

$$\frac{S_T}{S_L} = \frac{F_T}{F} \tag{2.15}$$

where $\rho_0$ is the reactant density, $S_T$ is turbulent flame speed and $F$ is the projected flame cross-sectional area.

For small scale turbulence Damköhler assumed:

$$S_L \sim (D/t_{chem})^{1/2} \tag{2.16}$$

$$S_T \sim (D_t/t_{chem})^{1/2} \tag{2.17}$$

where $t_{chem}$, $D$ and $D_t$ are chemical timescale, molecular diffusivity and turbulent diffusivity respectively. Moreover, the turbulent diffusivity, $D_t$, is proportional to the $u'l_t$, where $l_t$ is the integral length scale and $u'$ is the root mean square of the velocity fluctuations. The laminar diffusivity, $D$, is proportional to the $S_L\delta_L$, where $\delta_L$ is the flame thickness. Therefore:

$$\frac{S_T}{S_L} \sim \left(\frac{D_t}{D}\right)^{1/2} \sim \left(\frac{u'}{S_L}\frac{l_t}{\delta_L}\right)^{1/2} \tag{2.18}$$

Showing that for small scale of turbulence, the ratio of the turbulent to laminar flame speed also depends on the ratio of integral length scale to the flame thickness (Peters, 1999). Based on the relation 2.18, when $u'$ is very small, $S_T$ tends towards zero values. This is not true in real flames where for very small $u'$, $S_T$ is expected to tend towards $S_L$. In order to fix this problem, Abdel-Gayed *et al.* (1984) and Gülder (1990) have proposed relations between laminar and turbulent flame speed in the form:

$$\frac{S_T}{S_L} = 1 + fn\left(\frac{u'}{S_L}, l_t, \delta_L\right) \tag{2.19}$$

Equation 2.19 shows that premixed combustion is boosted by turbulent motions (Poinsot and Veynante, 2005). Initial interest in turbulent flames was concentrated on models for the turbulent flame speed and $S_T$ was the only parameter of concern. However, understanding of turbulent premixed flame behaviour depends on more than simply $S_T$.

## *2.5 Regimes in Turbulent Premixed Combustion*

For determining the flow regime in premixed turbulent combustion, a Borghi diagram (Borghi, 1984) is often used. The Borghi diagram defines combustion regimes in terms of length scale and velocity scale ratios. Figure 2.2 shows the different combustion regimes in Peters (1999) version of the Borghi diagram.

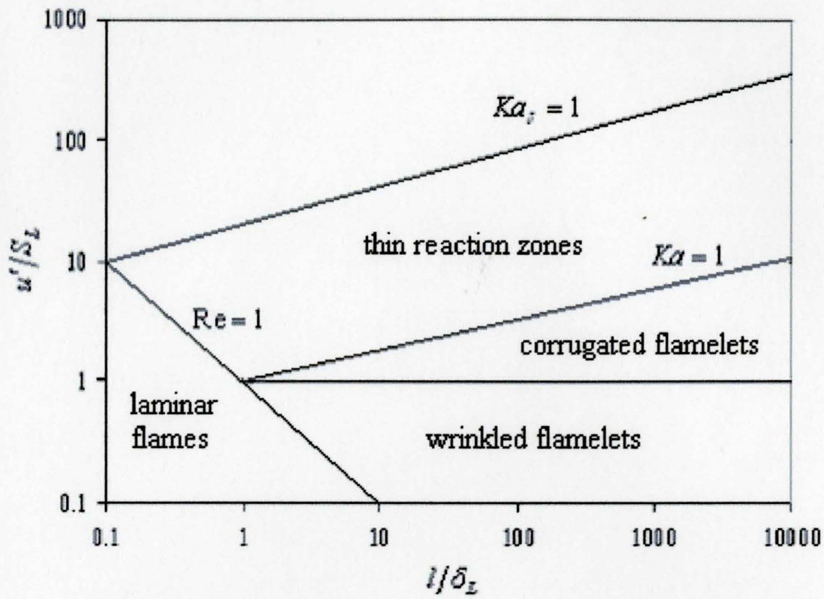


Figure 2.2: Regime diagram for turbulent premixed combustion (Peters, 1999).

The turbulent Reynolds number is defined as: (Poinsot and Veynante, 2005)

$$\mathrm{Re}_t = \frac{u'l_t}{\nu} = \frac{u'l_t}{S_L \delta_L} \tag{2.20}$$

The Karlovitz number is the ratio of chemical time/length scales to the smallest (Kolmogorov) turbulence scales:

$$Ka = \frac{t_{chem}}{t_k} = \frac{\delta_L^2}{\eta^2} \tag{2.21}$$

where $t_{chem}$ is time scale associated with flame chemistry and $t_k$ is Kolmogorov time scale.

An additional Karlovitz number for the inner layer thickness (reaction zone thickness) $\delta_R$ can be defined as:

$$Ka_\delta = \frac{\delta_R^2}{\eta^2} \tag{2.22}$$

When $Ka < 1$, the chemical time scale is shorter than the turbulent time scale. In this region, the flame is thin and has a structure close to that of a laminar flame. Turbulence can then wrinkle the flame, but turbulent eddies are too big to enter the flame inner structure. This thin flame regime is divided into two parts:

- Corrugated flamelet regime in which $\frac{u'}{S_L} > 1$. Turbulent eddies are able to wrinkle the flame enough that portions of the flame front can interact with each other. As a result, pockets of fresh and burnt gases are formed (Poinsot and Veynante, 2005).

- Wrinkled flamelet regime where $\frac{u'}{S_L} < 1$. The turbulent motion is not able to wrinkle the flame up to flame interactions (Poinsot and Veynante, 2005).

In the thin reaction zones regime ($\mathrm{Re} > 1$, $Ka > 1$ and $Ka_\delta < 1$), the flame preheat zone thickness is larger than the smallest turbulent scales (Kolmogorov scale) and the smallest eddies can enter into the flame structure and thicken the flame preheat zone. However, since $Ka_\delta < 1$, the smallest eddies are still larger the reaction zone.

At the top of the diagram, above the $Ka_\delta = 1$ line, the Kolmogorov scales are smaller than the inner layer thickness and they can enter to the inner layer of the flame. Both diffusion and reaction zones are mixed by the high turbulence level producing what is often referred to as distributed reactions.

In the present study, we are interested in thin flames in the corrugated and wrinkled flamelet zones where turbulent eddies cannot penetrate into the flame structure. In this case, the flame behaves like a laminar wrinkled flame and, consequently, simplified chemistry can be used. Since our study focuses on the effects of turbulence on the flame, resolving the three-dimensional turbulence field is regarded as paramount. For the thin reaction zones flames, simulations with complex chemistry would be necessary since the inner structure of the flame is changed by turbulent eddies.

## 2.6 *Previous Direct Numerical Simulations on Turbulent Premixed Flames*

Direct Numerical Simulation is a method of simulating flow by solving Navier-Stokes equations numerically without any modeling. Because of the accuracy of this method and the detailed flow field information provided, it has been a powerful method for studying turbulent flows. DNS has been widely used for turbulent premixed combustion. A survey of DNS for turbulent premixed flames is shown in table 2.1:

| Author(s) | Year | Chemistry | 2D/ 3D | Grid | Density | Re | Notes |
|---|---|---|---|---|---|---|---|
| Ashurst and Barr | 1983 | No/Arrhenius | 2D | | constant/ variable | | Study of premixed flame propagation via vortex dynamics. |
| Ashurst | 1987 | No | 2D | | constant | | Vortex simulation of unsteady wrinkled laminar flames in V-shape and bunsen burner flames. |
| Ashurst, Kerstein, Kerr, Gibson | 1987 | No | 3D | $128^3$ | constant | 83 (Taylor) | The alignment between vorticity and eigenvectors of the strain rate tensor using pseudospectral calculations. |
| Laverdant, Candel | 1989 | one-step Arrhenius | 2D | | constant | | Explored the interaction between a vortex and a premixed laminar flame. |
| Rutland, Ferziger | 1989 | one-step Arrhenius | 2D | | variable | | Study of the interaction of a vortex structure and a premixed flame. |
| Barr | 1990 | No | 2D | | variable | | |
| Yeung, Girimaji, Pope | 1990 | No | 3D | $128^3$ | constant | 38 to 93(Taylor) | Examined the straining on material surfaces and the behaviour of thin diffusive layers. |
| Cant, Rutland, Trouve | 1990 | one-step Arrhenius | 3D | $128^3$ | constant | | Extracted statistical information for laminar flamelet modeling. |

| | | | | | | | |
|---|---|---|---|---|---|---|---|
| Patnaik and Kailasanath | 1990 | Complex | 2D | | variable | | Study of the initiation and subsequent development of cellular structures in lean hydrogen-air flames. |
| El Tahry, Rutland, Ferziger | 1991 | one-step Arrhenius | 3D | $128^3$ | constant | 3.9, 9.2, and 18(Taylor) | Study of the local flame speed and structure of turbulent premixed flames. |
| Poinsot, Veynante, Candel | 1991 | one-step Arrhenius | 2D | 25000 points | variable | 0 to 3000 | Prediction of flame quenching by isolated vortices/effect of curvature and viscous dissipation on flame/vortex interactions/non-unity Lewis number. |
| Haworth, Poinsot | 1992 | one-step Arrhenius | 2D | $400^2$ | variable | 86, 88, 91 (integral) | Lewis number effects in turbulent premixed flames. |
| Rutland, Trouve | 1993 | one-step Arrhenius | 3D | $128^3$ | constant | 30 | The effect of turbulence on premixed flames in the flamelet regime. |
| Trouve, Poinsot | 1994 | one-step Arrhenius | 3D | $129^3$ | variable | 50(Taylor) or 70(integral) | Estimated the different terms appearing in the evolution equation of the flame surface density/Different Lewis numbers. |
| Rutland, Cant | 1994 | one-step Arrhenius | 3D | $251 \times 128 \times 128$ | variable | 30(scaling), 56.7 (integral) | Simulations of planar, premixed turbulent flames to study turbulent transport. |
| Baum, Poinsot, Haworth | 1994 | Complex | 2D | $301^2$/ $487^2$/ $601^2$ | variable | 275 to 959 (turbulent) | Studied H2/ O2/ N2 flame propagation in turbulent flow. |
| Kostiuk, Bray | 1994 | Complex | 2D | | constant | | Modeling the mean effects of stretch on laminar flamelets in a premixed turbulent flame. |
| Zhang, Rutland | 1995 | one-step Arrhenius | 3D | $129 \times 128 \times 128$ | variable | 30,20(scaling), 39,53 (turbulent) | Studied the flame effects on turbulence within the turbulent flame brush by examining the turbulent kinetic energy budget. |
| Dandekar and Collins | 1995 | one-step Arrhenius | 3D | $96^3$ | variable | 85 (Taylor) | Studied the effect of nonunity Lewis number on premixed flame in turbulent flow. |
| Echekki and Chen | 1996 | Complex | 2D | $501^2$ | variable | 135(integral), 36 (Taylor) | The effects of strain rate and curvature on the intermediate radical concentrations and heat release rate are evaluated for turbulent premixed stoichiometric methane-air flames. |
| Ashurst, Shepherd | 1997 | one-step Arrhenius | 3D | $64^3$ | variable | 55 (Taylor) | Compared distributions of flame front curvature obtained by laser sheet tomography with the numerical simulation results. |
| Chen, Im | 1998 | Complex | 2D | $750^2$ | variable | 181(integral) | Determined the correlation of flame-speed with stretch over a wide range of curvatures and strain rates for methane-air flames. |

| | | | | | | | |
|---|---|---|---|---|---|---|---|
| Peters, Terhoeven, Chen, Echekki | 1998 | Complex | 2D | | variable | | Statistics of flame displacement speed for premixed methane flames in thin reaction zone. |
| Chen, Echekki, Kollmann | 1999 | Complex | 2D | $750^2$ | variable | 181 (integral) | Performed a simulation on premixed lean methane-air flame to investigate the mechanism of unburnt pocket formation. |
| Cant | 1999 | one-step Arrhenius | 3D | 129 × 128 × 128 | constant | 50 (turbulent) | Examined the interaction of a premixed flame with a turbulent field. |
| Swaminathan, Bilger, Cuenot | 2001 | Complex | 2D | | variable | 598, 613, 289, 135 (turbulent) | Study of the behavior of the turbulent scalar flux in hydrogen-air and methane-air flames. |
| Jime´nez, Cuenot, Poinsot, Haworth | 2002 | Complex | 2D | $451^2$ | variable | 105 (turbulent) | DNS of lean non-homogeneous propane-air mixtures have been performed for several initial distributions of non-homogeneities. |
| Bell, Day, Grcar | 2002 | Complex | 3D | Adaptive grid | variable | 100 (turbulent) | Studied the behaviour of premixed turbulent methane flame |
| Tullis, Cant | 2002 | one-step Arrhenius | 3D | $96^3$ and 256 × 128 × 128 | variable | 25, 30 (integral) | Developed a LES SGS models by filtering the DNS results. |
| Chakraborty, Cant | 2003 | one-step Arrhenius | 3D | $96^3$ | variable | 25 (integral) | Studied strain rate and curvature effects on the flame displacement speed. |
| Hawkes, Chen | 2004 | Complex | 2D | 480 × 1200 | variable | 143 (integral) | Studied the effect of hydrogen blending on lean premixed methane–air flames. |
| Nada, Tanahashi, Miyauchi | 2004 | Complex | 3D | 257 × 256 × 256,513 × 128 × 128 | variable | 37.4 (Taylor) | Investigated effects of turbulence characteristics on the local flame structure of H2-air premixed flame. |
| Thevenin | 2005 | Complex | 3D | $146^3$ | variable | 74/167 | Investigated the structure of premixed methane flames expanding in a three-dimensional turbulent velocity field, initially homogeneous and isotropic. |
| Chakraborty, Cant | 2005 a | one-step Arrhenius | 3D | $96^3$ and $128^3$ | variable | 25, 30 (integral) | Effect of strain rate and curvature on surface density function transport. |
| Chakraborty, Cant | 2005 b | one-step Arrhenius | 3D | $96^3$ | variable | 25 (integral) | Influence of Lewis number on curvature effects in the thin reaction zone regime. |
| Chakraborty, Cant | 2006 | one-step Arrhenius | 3D | $96^3$ | variable | 25 (integral) | Influence of Lewis number on strain rate effects. |
| Hawkes, Chen | 2006 | Complex | 2D | 480 × 1200 | variable | | Studied statistics of displacement and consumption speeds in turbulent lean premixed methane–air flames. |
| Bell, Cheng, Day, Shepherd | 2007 | Complex | 2D | 160 × 320 to 1280 × 2560 (adaptive mesh) | variable | | Examined effects of Lewis number on lean premixed combustion. |

| | | | | | | | |
|---|---|---|---|---|---|---|---|
| Chakraborty | 2007 | one-step Arrhenius | 3D | 261 × 128 × 128 and $230^3$ | variable | 47, 56.7 (turbulent) | Comparison of displacement speed statistics in corrugated flamelets regime and thin reaction zones. |
| Chakraborty, Swaminathan | 2007 | one-step Arrhenius | 3D | 261 × 128 × 128 and $128^3$ | variable | 56.7, 41 (turbulent) | Studied the modeling of Damköhler number, Da, effects on the interaction of turbulence and scalar fields in premixed flames. |
| Chakraborty, Hawkes, Chen, Cant | 2008 | Complex | 2D | 480 × 1200 and 520 × 512 | variable | | The effect of strain rate and curvature on surface density function for methane-air and hydrogen-air flames. |

Table 2.1: Survey of previous direct numerical simulations of premixed turbulent flames.

Table 2.1 indicates improvements in both computational power and more advanced algorithms over time. Two-dimensional calculations which needs less grid point are replaced by three-dimensional domains. Early work during the 1980s and the beginning of the 1990s, often assumed constant density. Since resolving chemistry is computationally expensive, the early direct numerical simulations on premixed combustion started with considering no chemistry. In this case, DNS was used to study the propagation of a material surface in turbulent flows. Later, computations were performed using simple one-step chemistry with Arrhenius reaction rate. The use of complex chemistry is computationally expensive and often requires assuming two-dimensional turbulence to highly reduce the number of grid points (and so computational costs needed). As it is clear from the table, the value of Reynolds number is proportional to number of grid points and increasing computer power has allowed increasing Reynolds numbers. It is only very recently that three-dimensional DNS with complex chemistry have been performed and these are still at very modest Reynolds numbers.

The effect of curvature on flame tangential strain and displacement speed has been investigated extensively. Yeung *et al.* (1990) used three-dimensional direct numerical simulation of turbulence with constant density on non-reacting flows to examine the straining on material surfaces and the relationship between strain rate and curvature. The flame is seen to align mostly with positive (expansive) strains and near-zero average strains are experienced by high curved surfaces. Also, study of flame with no heat release has been done by Cant (1999) in order to examine the interaction of a premixed flame with a turbulent field. This study did not find any correlation between strain rate and curvature.

Two-dimensional DNSs of premixed flames with detailed chemistry have been carried out by Echekki and Chen (1996), Chen and Im (1998), Peters *et al.* (1998) and Hawkes and Chen (2006); and with one-step chemistry by Haworth and Poinsot (1992). Hawkes and Chen (2006) used DNS to study statistics of displacement and consumption speeds in turbulent lean premixed methane-air flames. A strong nonlinear relationship between displacement speed and curvature at negative curvatures was seen by Echekki and Chen (1996), Chen and Im (1998) and Peters *et al.* (1998) for turbulent premixed stoichiometric methane-air flames. They related this correlation to the coupling of curvature with differential diffusion effects of hydrogen atom in the reaction zone (Echekki and Chen, 1996 and 1999). However, this nonlinearity was seen in our results (see chapter 4) with single-step chemistry and so does not seem to be due to chemistry. According to Chen and Im (1998), the displacement speed is enhanced for large negative curvatures due to the differential diffusion and focusing of mobile radicals, and also by upstream flame–flame interaction. For a radius of curvature less than one thermal flame thickness, the flame thermo-diffusive and reactive layers start to merge into the neighboring flames. As a result, the flame accelerates due to vanishing species gradients and shifts in balance between chemical reaction and normal diffusion as cusps develop (Chen and Im, 1998) (Chen *et al.*, 1999). In addition, they observed positive mean value in the PDF of strain rate which was consistent with the previous computations with simple chemistry (Echekki and Chen, 1996).

Haworth and Poinsot's (1992) DNS showed probability density functions (PDFs) of flame curvatures are almost symmetric about a near-zero mean, while the flame aligns preferentially with extensive tangential strain rate. A strong correlation between the local tangential strain rate and the local curvature was found in their simulations. They believed that this curvature-strain rate correlation is a result of the asymmetry of turbulence (high in the pre-flame gases, low in the post flame regions), as well as specific features of the computation (Haworth and Poinsot, 1992). This idea is not compatible with our results where the same correlation between tangential strain rate and curvature is seen in the laminar sinusoidal flames.

Bell *et al.* (2007) examined the effects of Lewis number on lean premixed combustion primarily using two-dimensional simulations of hydrogen, methane and propane flames. They observed a strong negative correlation between flame local burning speed and curvature which is increased in regions of negative curvature. A similar but much weaker correlation was observed for the methane flame. However, for the hydrogen flame, a very strong positive correlation with positive curvature and a weaker positive correlation with negative curvature were seen.

Chakraborty and Cant (2003 and 2004) and Jenkins *et al.* (2006) investigated strain rate and curvature effects on the propagation and displacement speed of the turbulent planar premixed flames (Chakraborty and Cant, 2003 and 2004) and flame kernels (Jenkins *et al.*, 2006) using three-dimensional compressible DNS with single-step chemistry. They reported a negative correlation between tangential strain rate and curvature and displacement speed and mean curvature. They suggested that the correlation between strain rate and curvature could be due to the higher turbulence levels present ahead of the flame than behind it. Our results in chapter 4 show that even for a laminar flame, this correlation is observed. Their results also showed a very weak correlation between local displacement speed and local tangential strain rate. However, conditional joint PDF of displacement speed and tangential strain rate at zero curvature locations indicated a negative correlation between tangential strain rate and displacement speed (Chakraborty and Cant, 2003 and 2004). They also showed that, in the case of flame kernels, the magnitude of the reaction progress variable is negatively correlated with curvature. For the planar flames, this correlation is weak.

In 2005b, Chakraborty and Cant used the same simulations to investigate the influence of Lewis number on curvature effects. They found a negative correlation between dilatation and curvature as well as tangential strain rate and curvature. Dilatation and curvature were seen to have a stronger correlation than tangential strain rate and curvature. In the other paper in the same year (Chakraborty and Cant, 2005a) they studied the effect of strain rate and curvature on surface density function, $|\nabla c|$, transport. A positive correlation between surface density function (SDF) and tangential strain rate was shown. In their results, the joint PDF of SDF and curvature has two branches. For positive curvature, the correlation between SDF and curvature is negative. For negative curvature there is a weak positive correlation. This behavior was said to be a consequence of the correlation between strain rate and curvature together with the correlation between displacement speed and curvature (Chakraborty and Cant, 2005a).

Chakraborty and Cant (2006) also studied the influence of Lewis number on strain effects. Again a negative correlation between tangential strain rate and curvature was reported. They believed that this correlation is due to heat release and plays an important role in the response of displacement speed to tangential strain rate. It was also shown that the surface density function and tangential strain rate are positively correlated which demonstrates that the local flame thickness decreases with increasing tangential strain rate. In 2007, they used a similar simulation to compare the statistics for two combustion regime zones (Chakraborty, 2007): corrugated flamelets and thin reaction zones. Their results show that for a flame in the corrugated flamelets regime, the curvature and $|\nabla c|$ are mildly positively correlated, while for thin reaction zones flames, the joint PDFs between $|\nabla c|$ and curvature has one branch with positive correlation and the other one with negative correlation. A negative correlation between $S_d$ and curvature was seen which was linear for the corrugated flamelets and nonlinear for the thin reaction zones regimes.

Chakraborty *et al.* (2008) performed two-dimensional direct numerical simulations for lean methane-air and hydrogen-air flames using detailed chemistry. They investigated the effects of tangential strain rate and curvature on the surface density function. For both hydrogen and methane flames, dilatation and curvature were negatively correlated. However, this correlation is much weaker in the hydrogen flame than in the methane flame. This difference was explained to be because of the differential diffusion of heat and species (Chakraborty *et al.*, 2008). The correlation between the normalized tangential strain rate and normalized curvature remains negative throughout the flame brush for the methane flame, in contrast with the hydrogen flame where this correlation remains weak throughout the flame brush. Moreover, for the methane flame, the surface density function and curvature are mainly negatively correlated while for highly negative curvature the correlation is positive. In the hydrogen flame the overall correlation is positive (Chakraborty *et al.*, 2008).

Experimental investigations of flame strain rate and local flame properties such as curvature and displacement speed have also been done by Bradley *et al.* (2003), Renou *et al.* (1998) and Nye *et al.* (1996). These papers reported symmetry in PDFs of tangential strain rate with respect to a mean value near zero which is in contrast with most numerical simulation results (Haworth and Poinsot, 1992) (Kostiuk and Bray, 1992). Renou *et al.* (1998) also found a negative correlation between curvature and tangential strain rate for propane and methane-air flames.

Although simulations with higher Reynolds numbers and resolution exist, $256^3$ grid points, which is used here, is a typical and acceptable resolution compared to the other current three-dimensional premixed flame simulations. The previous studies on premixed combustion usually focused on tangential strain rate and displacement speed. There has been little work done on the flame dilatation and normal strain rate which are very significant in flame behaviour and combustion modeling. Different factors such as heat release and turbulence influence turbulent premixed flame and consequently its dilatation, strain and displacement speed. The effect of each factor has not been considered separately in the previous studies. In this work we try to isolate these effects in order to explore the flame behaviour more accurately.

# Chapter 3

# Numerical Details

Three dimensional direct numerical simulations (DNS) of premixed flames in a cube are performed using a fully compressible finite difference code (Jenkins and Cant, 1999). Four different cases are studied:

- An initially planar flame in a turbulent flow field.
- A laminar sinusoidal flame.
- Turbulent $\tau$=0 back to back flames.
- A laminar sinusoidal flame with peak of reaction rate in front of the flame.

The flames are inserted in a box with $x$-coordinate which is the direction of the propagation of the laminar flame and $y$ and $z$ for the other directions. Figure 3.1 shows the computational domain.

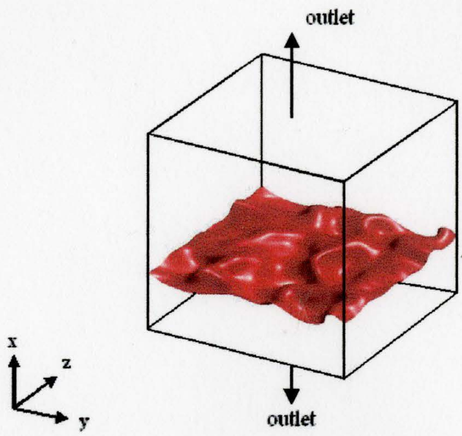


Figure 3.1: The computational domain with a flame surface shown in red.

### *3.1 Governing Equations*

The full set of governing equations for the compressible reacting flows in Cartesian tensor notation are given by:

The total mass conservation equation,

$$\frac{\partial \rho}{\partial t}+\frac{\partial(\rho u_k)}{\partial x_k}=0 \tag{3.1}$$

where $\rho$ is the density and $u_k(\vec{x},t)$ represents the $k$-th component of the fluid velocity at a point in space $x_k$ and time, $t$.

By neglecting external body forces acting on the flow, the conservation of momentum can be written as:

$$\frac{\partial(\rho u_i)}{\partial t}+\frac{\partial(\rho u_k u_i)}{\partial x_k}=-\frac{\partial P}{\partial x_i}+\frac{\partial(\tau_{ki})}{\partial x_k} \tag{3.2}$$

$P$ is pressure and $\tau_{ki}$ is the viscous stresses tensor, which assuming a Newtonian fluid, can be written as:

$$\tau_{ij} = \mu\left(\frac{\partial u_k}{\partial x_i} + \frac{\partial u_i}{\partial x_k} - \frac{2}{3}\delta_{ki}\frac{\partial u_m}{\partial x_m}\right) \tag{3.3}$$

where $\mu$ is the dynamic viscosity and $\delta_{ij}$ is Kronecker symbol.

By neglecting heat source terms (other than the combustion) and volume forces, the energy conservation equation reduces to:

$$\frac{\partial(\rho E)}{\partial t} + \frac{\partial(\rho u_k E)}{\partial x_k} = -\frac{\partial(P u_k)}{\partial x_k} + \frac{\partial(\tau_{ki} u_k)}{\partial x_i} - \frac{\partial q_k}{\partial x_k} \tag{3.4}$$

where $E$ is the stagnation internal energy and $q_k$ is the heat flux vector which is given by:

$$q_k = -\lambda\frac{\partial T}{\partial x_k} + \rho\sum_{\alpha=1}^{N} h_\alpha V_{\alpha k} Y_\alpha \tag{3.5}$$

where $T$ is the temperature, λ is the thermal conductivity, $h_\alpha$ is the enthalpy of formation of species $\alpha$, $V_{\alpha k}$ is the diffusion velocity of species $\alpha$ relative to the mixture and $Y_\alpha$ is the mass fraction of species $\alpha$.

### 3.1.1 Chemistry

The species conservation equation for $\alpha = 1,\ldots,N$ species is:

$$\frac{\partial(\rho Y_\alpha)}{\partial t} + \frac{\partial(\rho u_k Y_\alpha)}{\partial x_k} = \omega_\alpha - \frac{\partial(\rho V_{\alpha k} Y_\alpha)}{\partial x_k} \qquad \alpha = 1,\ldots,N \tag{3.6}$$

For the species mass fraction:

$$\sum_{\alpha=1}^{N} Y_\alpha = 1 \tag{3.7}$$

Resolving three-dimensional turbulence with complex chemistry is computationally costly. Consequently, the chemistry here is assumed to be a single-step irreversible reaction; this is possible because the flame is considered thin relative to the Kolmogorov length scale:

Reactant ➔ Product

By assuming that the mixture has only two species, reactants and products, a reaction progress variable can be defined as:

$$c = Y_P \tag{3.8}$$

By neglecting volume forces and assuming small pressure gradients, the diffusion velocity, $V$, in the progress variable equation obeys the Fick's law as following:

$$\rho V_{ck} c = -\rho D \frac{\partial c}{\partial x_k} \tag{3.9}$$

where $D$ is a diffusion coefficient and is a function of the local thermo-chemical state. Therefore equation 3.6 can be replaced by the conservation equation of reaction progress variable as follows:

$$\frac{\partial(\rho c)}{\partial t} + \frac{\partial(\rho u_k c)}{\partial x_k} = \frac{\partial}{\partial x_k}\left[\rho D \frac{\partial c}{\partial x_k}\right] + \dot{\omega} \tag{3.10}$$

For the reaction rate, the Arrhenius reaction rate is considered in the following form:

$$\dot{\omega} = B\rho(1-c)\exp\left[\frac{-E_a}{R^0 T}\right] \tag{3.11}$$

where $B$ is the pre-exponential factor and $E_a$ is activation energy.

The equations are closed using the equations of state:

$$P = \rho RT \tag{3.12}$$

$$E = C_V T + \frac{1}{2}u_k u_k + H(1-c) \tag{3.13}$$

where $C_V$ is the mixture specific heat capacity at constant volume and $H$ is the heat of reaction per unit mass of reactants consumed.

The heat flux vector can then be re-written as:

$$q_k = -\lambda \frac{\partial T}{\partial x_k} - \rho DH \frac{\partial c}{\partial x_k} \tag{3.14}$$

### 3.1.2 Non-dimensionalized Equations

The equations are non-dimensionalized by $u_0$, $l_0$, $t_0$, $\rho_0$ and $T_0$ where $u_0$ equals to laminar flame speed, $l_0$ is the domain size, $t_0 = l_0/u_0$ and $\rho_0$ and $T_0$ are initial reactants density and temperature respectively. The non-dimensional temperature is defined as:

$$T = \frac{\hat{T} - T_0}{T_{ad} - T_0} \tag{3.15}$$

$\hat{T}$ represents the instantaneous dimensional temperature, $T_0$ and $T_{ad}$ are initial and adiabatic flame temperatures, respectively. The internal energy is non-dimensionalized with respect to $C_{P_0} T_0$ and pressure is non-dimensionalized by $\rho_0 u_0^2$.

The non-dimensionalized forms of the governing equations are then:

$$\frac{\partial \rho}{\partial t} + \frac{\partial(\rho u_k)}{\partial x_k} = 0 \tag{3.16}$$

$$\frac{\partial(\rho u_i)}{\partial t} + \frac{\partial(\rho u_k u_i)}{\partial x_k} = -\frac{\partial P}{\partial x_i} + \frac{1}{\mathrm{Re}} \frac{\partial(\tau_{ki})}{\partial x_k} \tag{3.17}$$

$$\frac{\partial(\rho E)}{\partial t}+\frac{\partial(\rho u_k E)}{\partial x_k}=-(\gamma-1)Ma^2\frac{\partial(Pu_k)}{\partial x_k}+\frac{1}{\mathrm{Re}}(\gamma-1)Ma^2\frac{\partial(\tau_{ki}u_k)}{\partial x_i}$$
$$+\frac{\tau}{\mathrm{Re}\,\mathrm{Pr}}\frac{\partial}{\partial x_k}\left[\lambda\frac{\partial T}{\partial x_k}\right]-\frac{\tau}{\mathrm{Re}\,Sc}\frac{\partial}{\partial x_k}\left[\rho D\frac{\partial c}{\partial x_k}\right] \tag{3.18}$$

$$\frac{\partial(\rho c)}{\partial t}+\frac{\partial(\rho u_k c)}{\partial x_k}=\frac{1}{\mathrm{Re}\,Sc}\frac{\partial}{\partial x_k}\left[\rho D\frac{\partial c}{\partial x_k}\right]+\dot{\omega} \tag{3.19}$$

We close the equations by the two non-dimensional equations of state:

$$P=\frac{1}{\gamma Ma^2}\rho(1+\tau T) \tag{3.20}$$

$$E=\frac{1}{\gamma}(1+\tau T)+\frac{1}{2}(\gamma-1)Ma^2u_ku_k+\tau(1-c) \tag{3.21}$$

The ratio of specific heats, $\gamma$ and the heat release factor, $\tau$ are:

$$\gamma=\frac{C_{P_0}}{C_{V_0}} \tag{3.22}$$

$$\tau=\frac{\alpha}{(1-\alpha)}=\frac{(T_{ad}-T_0)}{T_0} \tag{3.23}$$

$C_{P_0}$ and $C_{V_0}$ are reactant heat capacities at constant pressure and volume respectively. The product temperature is assumed to be equal to the adiabatic flame temperature. $\alpha$ is the heat released by the flame.

The main non-dimensional parameters appearing in these equations are defined as:

Reynolds number: $\mathrm{Re}=\dfrac{\rho_0 u_0 l_0}{\mu_0}$ (3.24)

Prandtl number which compares momentum and heat transport is defined as:

$$\Pr = \frac{\nu_0}{D_{th_0}} = \frac{\nu_0}{\lambda_0/(\rho_0 C_{P_0})} = \frac{\mu_0 C_{P_0}}{\lambda_0} \tag{3.25}$$

where $\lambda_0$ is heat diffusion coefficient, $\mu_0$ is the dynamic viscosity and $D_{th_0}$ is the heat diffusivity coefficient.

The Schmidt number, Sc, compares momentum and molecular diffusion:

$$Sc = \frac{\nu_0}{D_0} = \frac{\mu_0}{\rho_0 D_0} \tag{3.26}$$

$D_0$ is the mass diffusion coefficient.

And Mach number: $Ma = \dfrac{u_0}{a_0}$ (3.27)

where $a_0 = \sqrt{\gamma R T_0}$ is the acoustic speed.

The chemical reaction rate is given by:

$$\dot{\omega} = B^* \rho (1-c) \exp\left[ -\frac{\beta(1-T)}{1-\alpha(1-T)} \right] \tag{3.28}$$

Heat released by the flame, $\alpha$, Zeldovich number, $\beta$ and the pre-exponential factor, $B^*$ are given as:

$$\alpha = \frac{\tau}{(1+\tau)} = \frac{T_{ad} - T_0}{T_{ad}} \tag{3.29}$$

$$\beta = \frac{E_a (T_{ad} - T_0)}{R^0 T_{ad}^2} \tag{3.30}$$

$$B^* = \frac{B}{\rho_0 u_0} \exp\left[-\frac{\beta}{\alpha}\right] \tag{3.31}$$

## 3.2 *Boundary Conditions*

The domain boundary conditions are periodic in the $y$ and $z$ directions and inflow-outflow in the $x$-direction using the Navier-Stokes characteristic boundary condition (NSCBC) (Poinsot and Lele, 1992). In the NSCBC method, at the boundaries, the Navier-Stokes equations are written in terms of locally one-dimensional inviscid equations that correspond to waves traversing the boundary with characteristic velocities. These are then solved in combination with an imposed physical boundary condition so that incident waves from inside the domain freely pass through the boundary and no waves are reflected.

## 3.3 *Numerical Schemes*

All first-order and second order derivatives are calculated using a 10th order explicit central difference scheme. As the boundaries are approached, the order of the scheme progressively decreases to 1$^{st}$ order. The equations are solved explicitly using a 3$^{rd}$ order low storage Runge-Kutta time marching scheme (Wray, 1990). The finite difference code was developed by Jenkins and Cant (1999). The code is parallelized using Message Passing Interface (MPI) by domain decomposition with a halo of five cells around each domain for message passing (Jenkins and Cant, 2001).

## 3.4 *Grid and Time Step Resolution for DNS*

Generally, for both reacting and non-reacting flows, the maximum Reynolds number which can be resolved by a DNS depends on the number of grid points. For resolving the turbulence scales, the largest and smallest scales need to be captured by the grid. The following shows the conditions for resolving the turbulent scales:

The Kolmogorov length scale (the size of smallest eddies) can be specified as:

$$\eta = (ul/\nu)^{-3/4} l_t = \mathrm{Re}^{-3/4} l_t \tag{3.32}$$

where $l_t$ is the integral length scale. This shows the inverse relationship between Reynolds number and Kolmogorov length scale. Since all eddies have to be resolved in a DNS, the number of grid points in the simulations are strongly dependant on the flow Reynolds number,

$$\Delta x \sim \eta \sim \mathrm{Re}^{-3/4} l_t \tag{3.33}$$

where $\Delta x$ is the maximum possible grid spacing.

For a DNS simulation:

$$N \sim \frac{L_{BOX}}{\Delta x} \sim \frac{L_{BOX}}{l_t} \mathrm{Re}^{3/4} \tag{3.34}$$

where $N$ is the number of data points required in each direction and $L_{BOX}$ is the computational domain size.

We can rewrite the above relation as:

$$\mathrm{Re} \sim \left( \frac{l_t}{L_{BOX}} \right)^{4/3} N^{4/3} \tag{3.35}$$

To be able to resolve the high Reynolds number flows, we need a vast number of data points which is computationally expensive.

For the code to be stable and accurate, an acoustic wave cannot move more than one grid spacing in one computational time step. According to Courant-Friedrichs-Levy (CFL condition), the possible time step needed for an explicitly solved compressible flow is limited by:

$$\Delta t \leq \Delta x / a_0 \tag{3.36}$$

where $a_0$ is the sound speed. The CFL number is defined as: $CFL = a_0\, \Delta t / \Delta x$. For explicit compressible codes, CFL number should be lower than unity.

$$\Delta t \leq \frac{\Delta x}{2} \frac{Ma}{u'} \tag{3.37}$$

The Mach number, *Ma*, was chosen such that the compressibility effects were minimized while not requiring excessively small time step from CFL condition.

Another condition for the DNS of a reacting flow is resolution of flame inner structure. This resolution highly depends on the type of chemical scheme used for DNS. For a single-step irreversible reaction, the inner structure of the flame should be resolved with at least ten to twenty grid points inside the flame (Poinsot *et al.*, 1996).

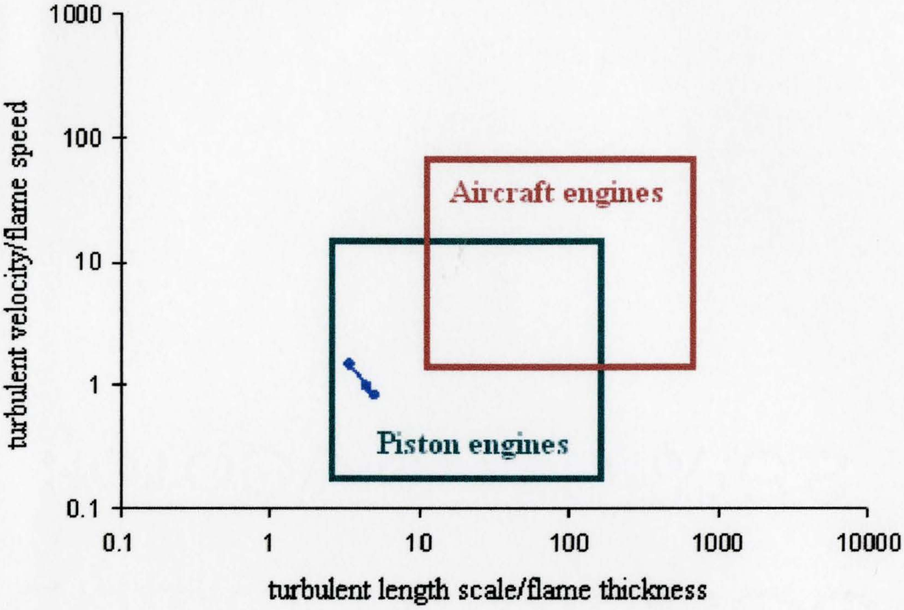


Figure 3.2: Practical applications of premixed flames on Borghi diagram (Poinsot and Veynante, 2005). The three blue points are turbulent cases resolved in this thesis in three different time steps.

This resolution requirement for the chemical scales makes a severe limitation for direct numerical simulations (Poinsot and Veynante, 2005). Figure 3.2 illustrates the Borghi diagram and the ranges of two practical applications, piston engines and gas turbine aircraft engines. Reynolds number (and hence resolution of the Kolmogorov length scale) and resolution requirements of the flame inner structure respectively limit the vertical and horizontal axis ranges of the simulations. The three blue points on the diagram indicate the turbulent premixed flame in this study at three different time steps (The initial flame at $t$=0, and the flame as examined at $t$=0.08 and $t$=0.16). It is seen that our case overlaps with some practical applications. The top point shows the initial flame. As time progresses, turbulence decays and integral length scale increases so the points move down and towards the right side of the diagram.

### 3.5 *Turbulent Flame*

An initially planar laminar flame is inserted into the turbulent flow field in a cube of unit volume. A three-dimensional, random, decaying, isotropic, homogeneous turbulent velocity field with periodic boundaries on all sides is considered with Batchelor-Townsend energy spectrum (Batchelor and Townsend, 1948) and imposed using the pseudo-spectral method developed by Rogallo (1981). This initial velocity field is incompressible, divergence-free and periodic in all three spatial directions. The initial energy spectrum is defined as:

$$E(\kappa) = \begin{cases} \gamma_E \kappa^2 & \kappa_{min} \leq \kappa \leq \kappa_{peak} \\ \gamma_E \kappa_{peak}^{\;2} \, (\kappa/\kappa_{peak})^{-5/3} & \kappa_{peak} \leq \kappa \leq \kappa_{max} \\ 0 & \text{otherwise} \end{cases} \tag{3.38}$$

where $\gamma_E$ is a constant determines the initial kinetic energy, $\kappa_{min}$ is the minimum non-zero wave number, $\kappa_{max}$ is the maximum wavenumber and $\kappa_{peak}$ is the wavenumber corresponding to the peak in the energy function spectrum.

The turbulent premixed flame is initialized using a pre-computed laminar flame with a non-dimensionalized laminar flame speed equal to 0.84. This velocity is obtained by changing $B^*$ and the Prandtl and Schmidt numbers. A uniform $256^3$ grid is used to resolve both turbulence and flame structure. The flame is resolved over 15 grid points. Initially, a laminar premixed flame case and a cold turbulent flame case were run for a small number of time steps. The laminar flame's progress variable profile and its associated temperature and density fields were imposed as an initial condition for turbulent premixed flame; while the velocity and energy fields of cold turbulent and laminar flame were added together.

Results from two different snapshots of the simulation are discussed in chapter 4. Tables 3.1 and 3.2 show the parameters used for the simulation and turbulence generation energy function spectrum. Table 3.3 indicates the resultant parameters from initially imposed turbulent flame and from two later time steps. Both flame and turbulence parameters showed in table 3.3 indicate that the flame is mostly located in the corrugated flamelet regime. As time progresses, turbulence decays and integral length scale increases. As a result, relative turbulence intensity declines while there is an increase in relative turbulent length scale and Bray number.

| | |
|---|---|
| Heat release factor, $\tau$ | 5 |
| $\alpha=\tau/(1+\tau)$ | 0.833 |
| Zeldovich number, $\beta$ | 4 |
| Pre-exponential factor, $B^*$ | 2500 |
| Ratio of specific heats, $\gamma$ | 1.4 |
| Reynolds number, $Re=1/\nu$ | 360 |
| Mach number, $Ma$ | 0.014159 |
| Prandtl number, $Pr$ | 0.2 |
| Schmidt number, $Sc$ | 0.2 |
| Lewis number, $Le$ | 1 |
| Grid spacing, $\Delta x$ | 0.0039 |
| Time step, $\Delta t$ | $2\times10^{-6}$ |

Table 3.1: Specified parameters used for the turbulent flame case.

| | |
|---|---|
| Initial kinetic energy constant, $\gamma_E$ | $2\times10^{-4}$ |
| Minimum wavenumber, $\kappa_{min}$ | $1\times2\pi$ |
| Maximum wavenumber, $\kappa_{max}$ | $100\times2\pi$ |
| Peak wavenumber, $\kappa_{peak}$ | $3\times2\pi$ |

Table 3.2: Initial energy function spectrum parameters.

| | Initially imposed | Time 0.08 | Time 0.16 |
|---|---|---|---|
| Heat release factor, $\tau$ | 5 | 5 | 5 |
| Laminar flame speed, $S_L$ | 0.84 | 0.84 | 0.84 |
| Laminar flame thickness, $\delta_L$ | 0.06 | 0.06 | 0.06 |
| Relative turbulence intensity, $u'/S_L$ | 1.45 | 1.11 | 0.93 |
| Relative turbulence length scale, $l_t/\delta$ | 3.4 | 4.5 | 5 |
| Bray number, $\tau S_L/2u'$ | 1.71 | 2.25 | 2.68 |

Table 3.3: Resultant parameters in two different snapshots of the simulation.

### *3.6 Laminar Sinusoidal Flame*

To isolate the effect of turbulence on the flame, a sinusoidal flame is made and inserted in a laminar flow. The flame parameters are as table 3.1. The initial sinusoidal shape was generated by specifying an initial displacement as following:

$$xdisp(y,z) = \sum_{i=1}^{9} A_i\left[\sin(2\pi\omega y) + \sin(2\pi\omega z)\right] \quad (3.39)$$

where $\omega$ is the wavenumber and $A_i$ is based on the turbulence imposed energy function spectrum as:

$$A_i = C\sqrt{E(k_i)} = \begin{cases} C\sqrt{\gamma_E k_i^2} & \kappa_{min} \le \kappa_i \le \kappa_{peak} \\ C\sqrt{\gamma_E k_{peak}^2\left(\dfrac{k_i}{k_{peak}}\right)^{-5/3}} & \kappa_{peak} \le \kappa_i \le \kappa_{max} \end{cases} \quad (3.40)$$

where $C$=0.1 specifies the overall amplitude of the initial sinusoidal shape.

### *3.7 Turbulent $\tau$=0 Flame*

In order to isolate the effect of heat release and gas dilatation, a turbulent case with zero heat release factor ($\tau$=0) is performed. There is no density changes across the flame as $c$ and $T$ go from 0 to1. The flame still propagates towards the reactants due to reaction but since there is no dilatation, it does not have any effect on the turbulent flow field. The flame properties such as laminar flame speed, flame thickness and reaction rate profile are same as the previous case. All turbulent properties are same as the turbulent case in part 3.5. The configuration used here was of two back to back planar flames in the initial turbulent field.

### *3.8 Laminar Sinusoidal Flame with a Different Reaction Rate Profile*

In this case, we want to examine the effect of reaction rate profile on flame structure. Hence, a similar case to the laminar sinusoidal flame, which was explained in section 3.6, is run but with a different reaction rate profile. The initial wrinkling of the flame is the same as part 3.6. Figure 3.3 shows the reaction rate profiles for the laminar sinusoidal flames in sections 3.6 and 3.8. As seen from the figure, in the present case the reaction rate profile peak is located in front of the flame close to reactants at $c$=0.32 but in the original flame, the peak is close to products at approximately $c$=0.8. To maintain the same laminar flame speeds in these two cases, the peak value for the reaction rate profile has been decreased while the general profile is broader compared to the original flame. The laminar flame speed is 0.93, very close to that of the previous flame.

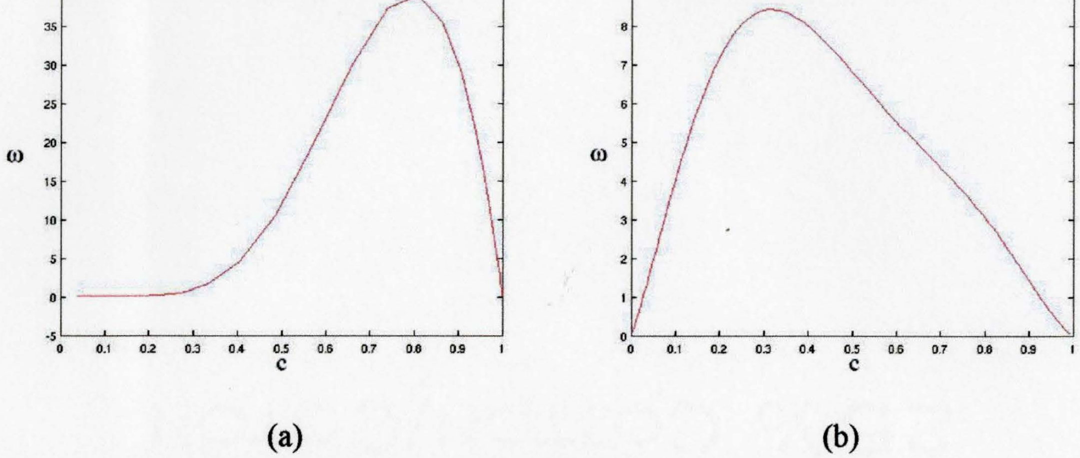


Figure 3.3: Variations of reaction rate versus progress variable. (a) Laminar sinusoidal flame in part 3.6. (b) Laminar sinusoidal flame in part 3.8.

# Chapter 4

# Results and Discussion

### *4.1 Turbulent Flame*

Here, a single laminar flat flame in the corrugated regime is inserted into a turbulent field. The main parameters of this simulation are: a heat release factor $\tau$=5, laminar flame speed, $S_L$=0.84, $u'/S_L$ =1.45 and a laminar flame thickness of 0.06. The Arrhenius reaction rate profile used has a peak of reaction rate located at $c$=0.8.

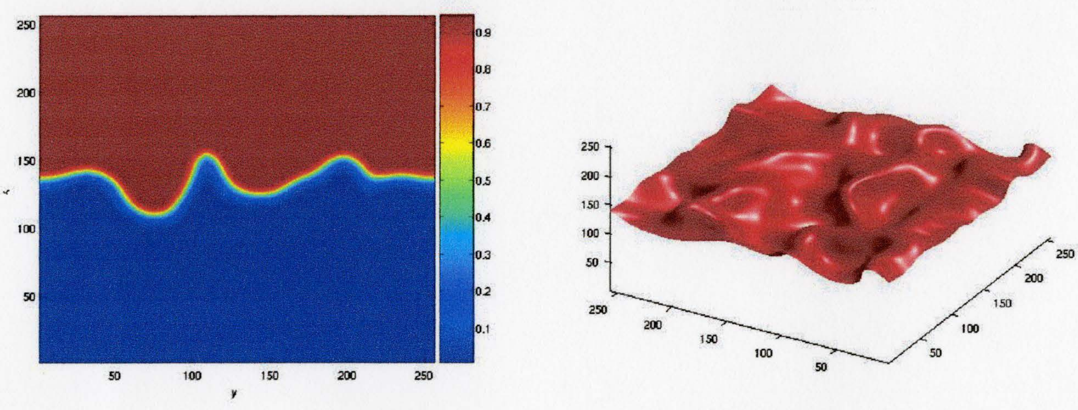

(a)

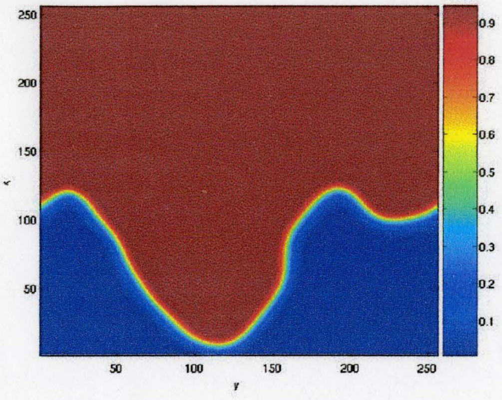

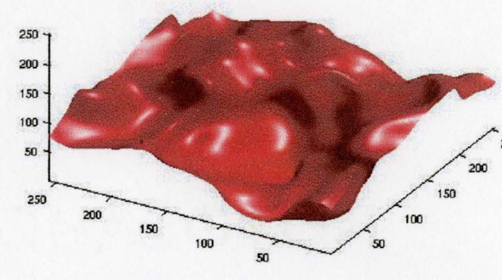

(b)

Figure 4.1: Contours of reaction progress variable in the $x$-$y$ plane at $z$=0.5 (Reactants are located at the bottom of the domain and are shown in blue. Products are in red and are at the top of the domain. The flame propagates towards the bottom of the domain into the reactants) and three-dimensional view of the flame on a progress variable isosurface, $c$=0.8: (a) $t$=0.08 (b) $t$=0.16.

Here, two time instances from the results are considered in detail; one fairly early in the simulation and the second after the turbulence has decayed significantly. Figure 4.1 shows the contours of reaction progress variable in the $x$-$y$ plane at $z$=0.5 and a three-dimensional view of the flame at $c$=0.8 isosurface for these two snapshots. In the early time steps, small eddies of turbulence have significant energy which wrinkles the initially laminar flame. In this stage, the wrinkles are small as seen in figure 4.1a. As time progresses, the smaller scales of turbulence dissipate and the size of the main energy containing eddies increases. The wrinkles then grow as they are convected by the turbulent eddies and their wavelength increases. The thin flame here behaves like a laminar wrinkled flame. There is no disruption of the flame profile ($c$-contours) by the turbulence. As the wrinkled flame propagates normal to itself into the reactants, the negatively curved regions (concave towards reactants) become more highly curved than regions of positive curvature (concave towards products). Figure 4.2 shows the evolution of a wrinkled flame front with time and the formation of these highly curved 'cusps', an effect known as Huygen's propagation. Cusp development and sharpening with time is also seen in figure 4.1. Regions of positive curvature, which do not sharpen, are often referred to as 'bulges'.

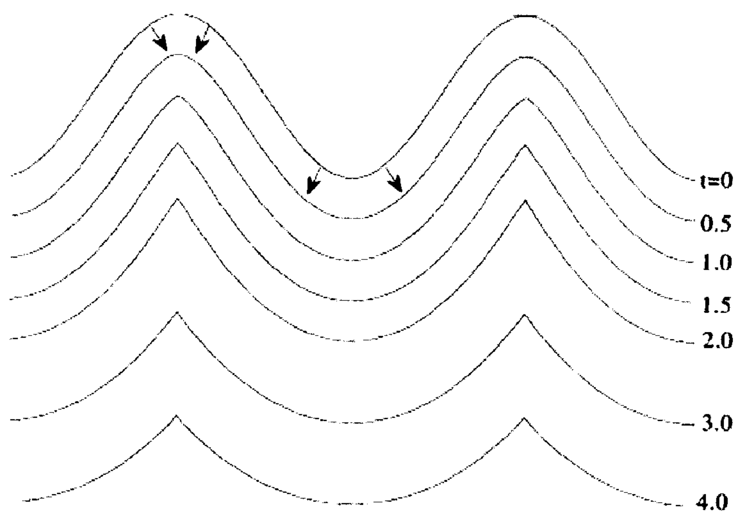


Figure 4.2: Evolution and propagation of an initially sinusoidal flame surface and the formation of cusps over the flame surface. (Modified from Law and Sung, 2000)

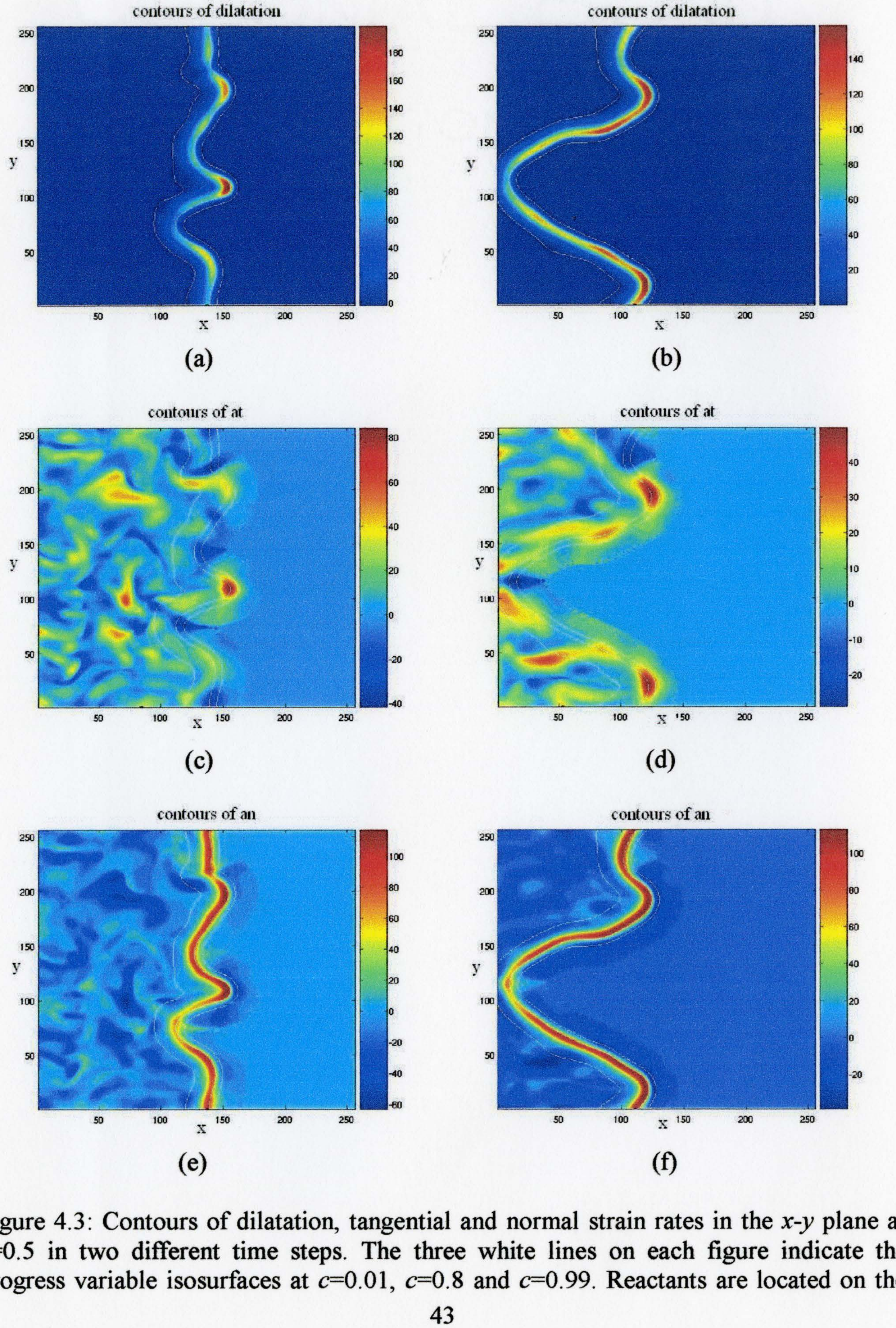


Figure 4.3: Contours of dilatation, tangential and normal strain rates in the $x$-$y$ plane at $z$=0.5 in two different time steps. The three white lines on each figure indicate the progress variable isosurfaces at $c$=0.01, $c$=0.8 and $c$=0.99. Reactants are located on the

left and products on the right side of the domain. (a) Dilatation ($\nabla.u$) at $t$=0.08 and (b) $t$=0.16. (c) Tangential strain rate ($a_t$) at $t$=0.08 and (d) $t$=0.16. (e) Normal strain rate ($a_n$) at $t$=0.08 and (f) $t$=0.16.

Contours of dilatation for the turbulent case in the $x$-$y$ plane in the middle of domain are plotted in figure 4.3a and 4.3b. Higher amounts of dilatation can be seen where the flame is convex towards products or in negative curvatures while the dilatation is lower in positively curved regions.

Figures 4.3c and 4.3d show the contours of tangential strain rate in the $x$-$y$ plane in the middle of domain for the two different time steps. The peak values of tangential strain rate decline as turbulence decays. Inside the flame, the highest positive values of tangential strain rate are in negative curvature regions or cusps. In bulges, where the curvature is positive, tangential strain rate is negative or compressive. Zero tangential strain rate is associated with flat or zero curvature regions. The tangential strain rate is only relevant inside the flame. The non-uniform values of $a_t$ in the reactants are simply due to turbulence. The flame tangential direction (normal to $\nabla c$) will have a meaningless value outside of the flame. The turbulence is damped on products side of the flame and flow velocity becomes more uniform so, the tangential strain rate is much reduced.

Figures 4.3e and 4.3f show that $a_n$ in the $x$-$y$ plane and in the middle of the domain remains positive throughout the flame brush. The highest value of normal strain rate can be seen on the isosurface of reaction rate peak, where $c$=0.8. On this isosurface, the normal strain rate does not appear to vary significantly with curvature.

The probability density functions (PDF) of curvature, dilatation, tangential strain rate and normal strain rate are plotted in figure 4.4 for the two different time steps.

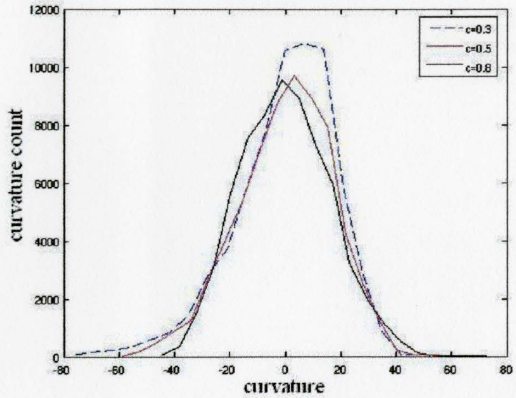
c=0.3
c=0.5
c=0.8
curvature count
curvature

(a)

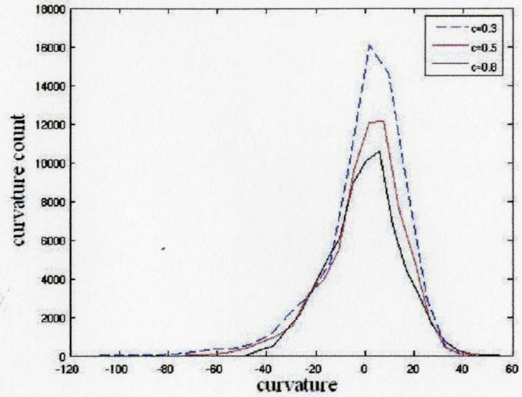
c=0.3
c=0.5
c=0.8
curvature count
curvature

(b)

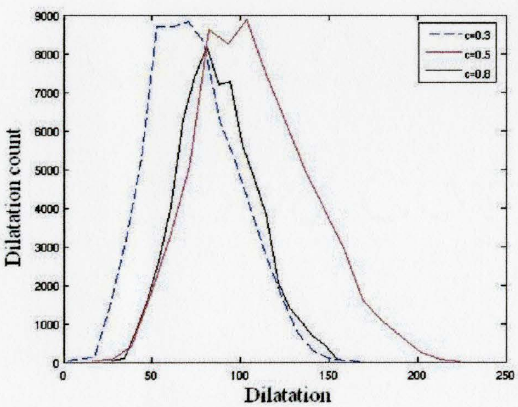
c=0.3
c=0.5
c=0.8
Dilatation count
Dilatation

(c)

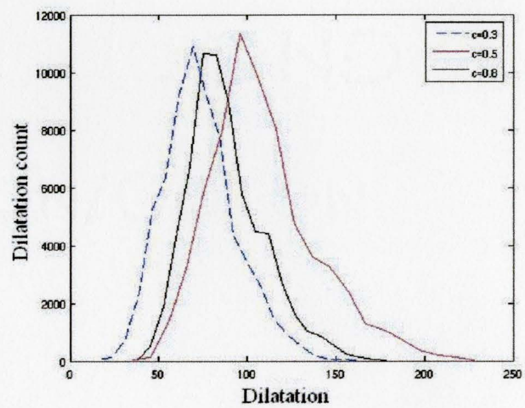
c=0.3
c=0.5
c=0.8
Dilatation count
Dilatation

(d)

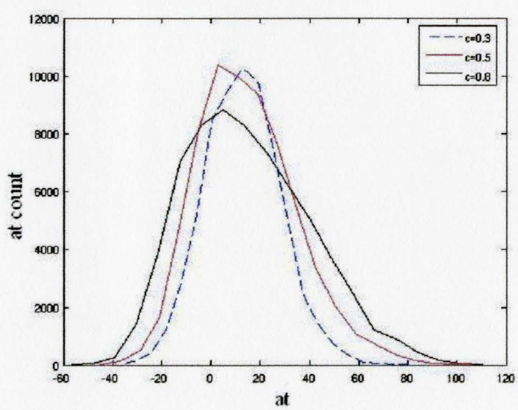
c=0.3
c=0.5
c=0.8
at count
at

(e)

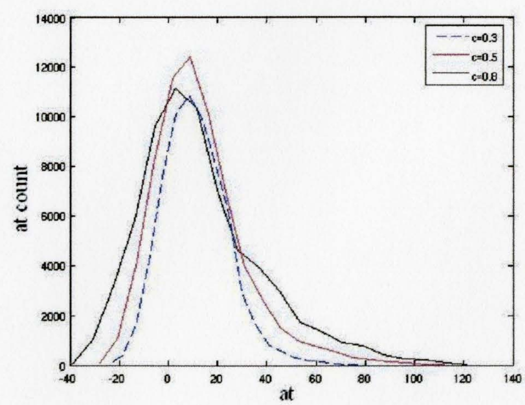
c=0.3
c=0.5
c=0.8
at count
at

(f)

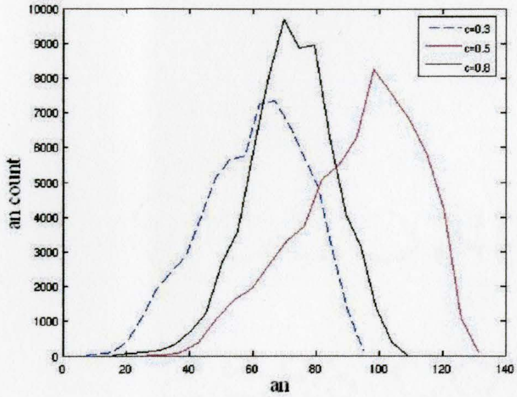


(g)

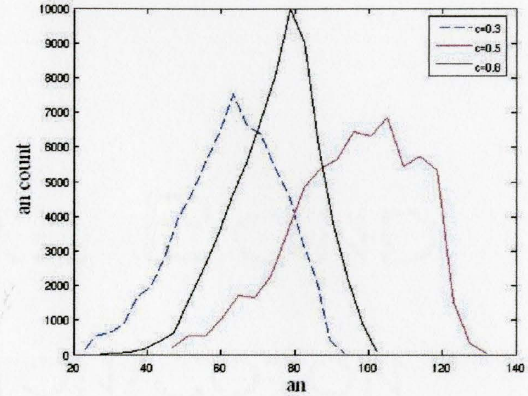


(h)

Figure 4.4: PDFs of curvature, dilatation, tangential and normal strains on three different progress variable isosurfaces (dash blue line: $c$=0.3, red line: $c$=0.5 and black line: $c$=0.8) in two different time steps. (a) Curvature at $t$=0.08 and (b) $t$=0.16 (c) Dilatation ($\nabla.u$) at $t$=0.08 and (d) $t$=0.16 (e) Tangential strain rate ($a_t$) at $t$=0.08 and (f) $t$=0.16 (g) Normal strain rate ($a_n$) at $t$=0.08 and (h) $t$=0.16. (counts are used instead of probabilities)

As seen from figure 4.4a, the PDF of curvature at $t$=0.08 is roughly symmetric about zero. Cusp formation is seen in significant counts at high negative curvatures. The similarity in the PDFs of curvature for different isosurfaces shows that the flame wrinkles due to turbulence are fairly uniform through the flame and that the flame is then behaving as a wrinkled laminar flamelet. On the reactant side of the flame ($c$=0.3 isosurface), there is more bulges area and there is a higher negative curvature on this surface compared to the product side ($c$=0.8). The combination of high curvature cusps and lower curvature bulges produces the small discrepancies between $c$ isosurface PDFs. There is simply more flame area on the reactant side of the flame (due to the low bulge curvature), and there are higher negative curvatures on this isosurface. At $t$=0.16, as seen from figure 4.4b, this behaviour is increased, the cusps sharpen and values of negative curvatures increase compared to $t$=0.08.

Figure 4.4c shows the PDF of dilatation at $t$=0.08. It is seen that higher values of dilatation occur on the $c$=0.5 than the $c$=0.3 and $c$=0.8 surfaces. Based on the contours of dilatation on an $x$-$y$ plane (figures 4.3a and 4.3b), and by looking at PDF results, it appears like the peak values of dilatation occur in a narrow region on the reactant side of the isosurface with the highest reaction rate (at approximately $c$=0.7 to $c$=0.75). These results are consistent with those of Swaminathan *et al.* (1997) where a single irreversible reaction rate with high activation energy was used but they disagree with Swaminathan *et al.* (2001) observations with complex chemistry where the peak of reaction rate and dilatation are not located at the same place. The PDF of dilatation at $t$=0.16 is very similar to $t$=0.08 and follows the same trend.

The PDF of tangential strain rate at $t$=0.08 (figure 4.4e) shows the skew of tangential strain rate to positive values with an obvious tail at very high positive values of $a_t$. This is consistent with the results of Yeung *et al.* (1990) and Girimaji and Pope (1992) on alignment of material and propagating surfaces with positive tangential strain rates. By comparing these results with contours of tangential strain rate on a slice at $x$-$y$ plane (figure 4.3c and 4.3d), it can be noted that these values of high positive tangential strain rate may occur at the cusps. There is a bigger range of tangential strain rate on $c$=0.8 isosurface where the peak of reaction rate occurs rather than $c$=0.3. At $t$=0.16, very large positive values of tangential strain rate increase.

As it is seen from figures 4.4g and 4.4h, unlike tangential strain rate, there is only positive flame normal strain rate. At the peak reaction rate location ($c$=0.8), $a_n$~70 with a roughly symmetric distribution. Like the dilatation, the values of normal strain rate are higher for the $c$=0.5 isosurface and lower for $c$=0.3. Based on the contours of normal strain rate on an $x$-$y$ plane, the peak values of normal strain rate appear to occur at $c$=0.7-0.75. Similar trend is seen for PDF of normal strain rate at $t$=0.16.

From PDF results and contour plots explained above, it can be seen that the contours of dilatation and normal strain rate are almost parallel to contours of reaction progress variable. Since $c$=0.8 isosurface follows the trend of dilatation and normal strain rate, it is suitable to explore the results on this isosurface. In the rest of this section, the joint PDFs of flame properties (dilatation, tangential strain rate, normal strain rate) and curvature are plotted on isosurface of $c$=0.8 and discussed. These are seen in figure 4.5 for $t$=0.08 and $t$=0.16. A strong linear relationship between dilatation and curvature can be clearly seen. The linearity is preserved over time. The curve bends slightly upwards (higher dilatation values) at minimum and maximum values of curvature.

For tangential strain, a negative correlation between tangential strain rate and curvature is seen in figures 4.5c and 4.5d. At the bulges, which have positive curvature, a negative or compressive tangential strain rates are seen, while cusps are associated with highly positive (expansive) tangential strain rates. The negative correlation was also reported in the previous studies. (Chakraborty and Cant, 2004, 2005b and 2006) (Chakraborty, 2007) (Chakraborty *et al.*, 2008). The correlation between the tangential strain rate and curvature is not as linear as the dilatation relationship with curvature. The tangential strain rate increases faster at very low negative curvatures. The nonlinearity increases by time as it is seen in figure 4.5d. Zero curvatures are associated with zero tangential strain rates. Much more of the joint PDF shows positive values of tangential strain rate which indicates the alignment of the flame surface with expansive tangential strain rates as was shown in PDF plots of $a_t$ (figures 4.4e and 4.4f). Around zero curvature regions, higher scatter in tangential strain rate is clear from figures 4.5c and 4.5d.

As seen from figures 4.5e and 4.5f, there is not an obvious strong correlation between normal strain rate and curvature. However at $t$=0.16, a decline in normal strain rate can be seen for very negative curvatures (cusps). For both time steps, normal strain rate values remain positive everywhere. There is a considerable scatter in $a_n$ especially at zero curvatures. .

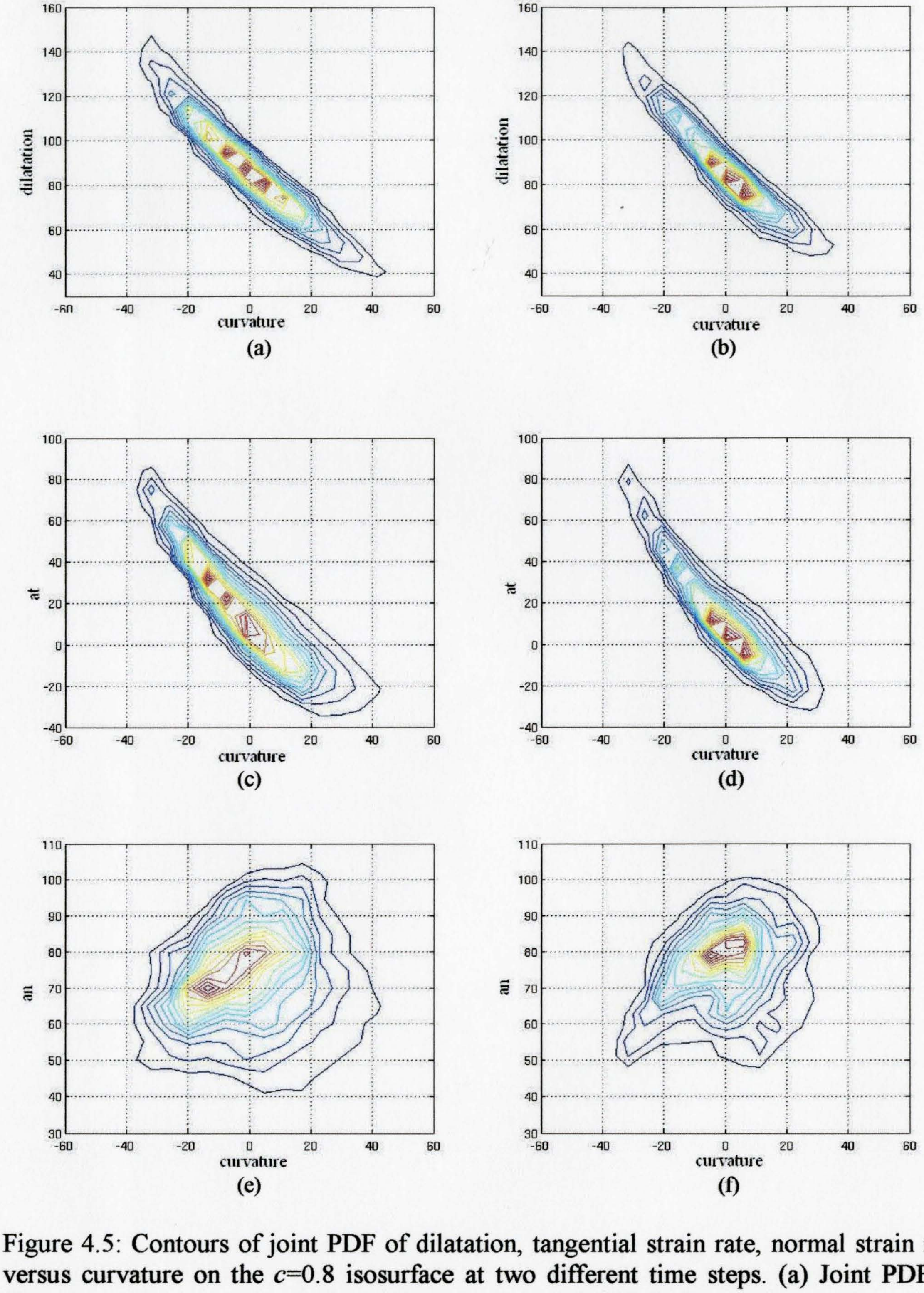


Figure 4.5: Contours of joint PDF of dilatation, tangential strain rate, normal strain rate versus curvature on the $c$=0.8 isosurface at two different time steps. (a) Joint PDF of dilatation and curvature, $t$=0.08 and (b) $t$=0.16. (c) Joint PDF of tangential strain rate and

curvature, $t$=0.08 and (d) $t$=0.16. (e) Joint PDF of normal strain rate and curvature, $t$=0.08 and (f) $t$=0.16.

The joint probability density functions of displacement speed and $|\nabla c|$ versus curvature for $t$=0.16 are plotted in figures 4.6a and 4.6b respectively.

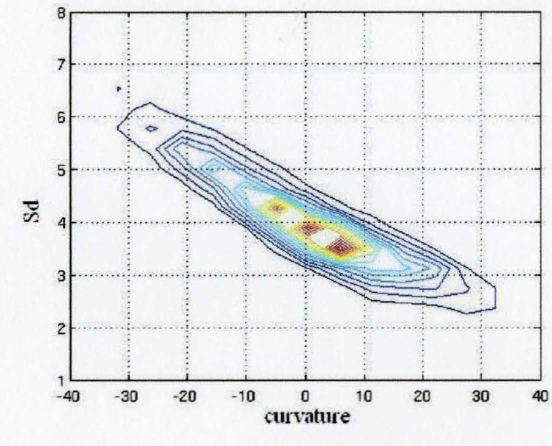


(a)

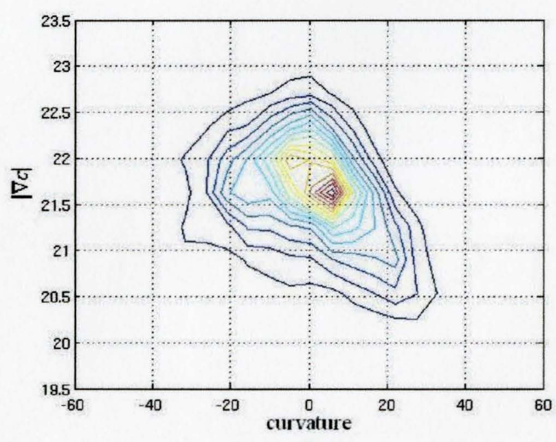


(b)

Figure 4.6: Contours of joint PDFs of displacement speed and $|\nabla c|$ versus curvature on the $c$=0.8 isosurface at $t$=0.16. (a) Joint PDF of displacement speed and curvature. (b) Joint PDF of $|\nabla c|$ and curvature.

Figure 4.6a shows that displacement speed is almost linear with curvature. Positively curved regions have lower displacement speed compared to negative curvature regions. This correlation is consistent with previous results of 2D and 3D numerical studies (Chen and Im, 1998) (Bell *et al.*, 2007) (Chakraborty and Cant, 2004, 2005a and 2005b) (Chakraborty, 2007). The small scatter is clear in the joint PDF of $S_d$ and curvature. The negative correlation between $S_d$ and curvature has been explained as due to the divergence of flow streamlines which occurs at negative curvature regions distributing the larger amount of reactants over a large flame surface. Consequently, a higher flux of reactants is burned and the displacement speed increases (Poinsot *et al.*, 1992). Moreover, flame tangential "leakage" of reactants by diffusion makes the reactant pathlines diverge faster than the streamlines of the mean flow and enhances the displacement speed further (Poinsot *et al.*, 1992). The same effect is also referred to as focusing (defocusing) of heat in the negatively (positively) curved regions leading to an increase (decrease) in $S_d$. For very large negative curvatures (cusps), $S_d$ is enhanced by upstream flame-flame interaction (Chen and Im, 1998). When the radius of curvature reaches the flame thickness, the flame preheat zone starts to interact with the adjacent flame so reactant heating is increased, leading to flame acceleration (Chen and Im, 1998).

The joint PDF of $|\nabla c|$ and curvature is essentially flat (the flame thickness is uniform) with a weak negative correlation for positive curvatures. Chakraborty (2007) reported a slightly positive correlation between curvature and $|\nabla c|$ in the corrugated flamelet zones. For negative curvatures, the value of $|\nabla c|$ is essentially constant. At the cusps themselves, the leading edge of the flame has higher negative curvature than the trailing edge. This can be seen from figures 4.4a and 4.4b where in $c$=0.3 isosurface, a higher negative curvature can be seen compared to $c$=0.8 isosurface. The negative correlation of $S_d$ and curvature which is linear at negative curvatures makes the flame thicker at cusps (Chakraborty and Cant, 2005a) and consequently, reduces $|\nabla c|$.

Based on relation 2.13, dilatation is proportional to the product of $S_d$ and $|\nabla c|$. The thin flamelet here is barely affected by turbulence or flame curvature (the value of $\nabla c|_{c=0.8}$ varies by less than 10%). So the negative correlation between dilatation and curvature can mostly be related to the effect of curvature on the displacement speed. As discussed earlier and is seen from figure 4.6a, $S_d$ is roughly linear with curvature.

As mentioned before, a negative correlation between tangential strain rate and curvature is seen in figures 4.5c and 4.5d. Divergence (convergence) of the flow streamlines in regions of negative (positive) flame curvature due to heat release (Poinsot *et al.*, 1992), cause a positive or expansive (negative or compressive) tangential strain rate which results to the negative correlation between $a_t$ and curvature. At the same time, it is expected that the turbulence will stretch the flame and cause the flame to align with positive tangential strain rates. The results also show that $a_t$ does not have the same linear relationship with curvature as the dilatation, with $a_t$ increasing more rapidly at large negative curvatures. This nonlinearity increases with time and appears to be related to the curvature approaching the scale of the flame thickness. The minimum radii of cusps are in the order of the laminar flame thickness (Haworth and Poinsot, 1992).

In summary, dilatation is a function of displacement speed and its behaviour with curvature is related primarily to the displacement speed dependency on curvature. There are two mechanisms relating $a_t$ with curvature, one due to the flame surface aligning with the turbulent strains, and the second due to heat release across the curved surface. Since the flame tangential and normal strain rates are just the two components of dilatation, $a_n$ can be explained in terms of differences between dilatation and tangential strain rate and the effect of curvature on each of them.

In order to isolate the effect of turbulence and flame heat release, two separate cases have been run. The first case is a laminar flow with the same flame properties as the original case, but with an initially wrinkled flame and the second case has the same turbulent properties as the original case but with zero heat release (constant density).

### *4.2 Laminar Sinusoidal Flame*

The flame tangential strain rate has two sources: alignment of a surface with the principal turbulent stresses and heat release/dilatation across curved flames. Since it is expected that the second of these is primarily responsible for the flame tangential strain behaviour seen here, a simplified DNS run was performed using the identical flame parameters, but introduced with a specified sinusoidal perturbed shape into an initially stagnant (laminar) velocity field. The initial flame thickness and laminar flame speed and other flame properties are same as the turbulent flame discussed in 4.1.

Figure 4.7 shows the flame curvature on an isosurface of $c$=0.8 (which is the peak reaction rate location) at $t$=0.16. The flame rapidly develops a cusped shape, and the curvature at the cusps increases with time.

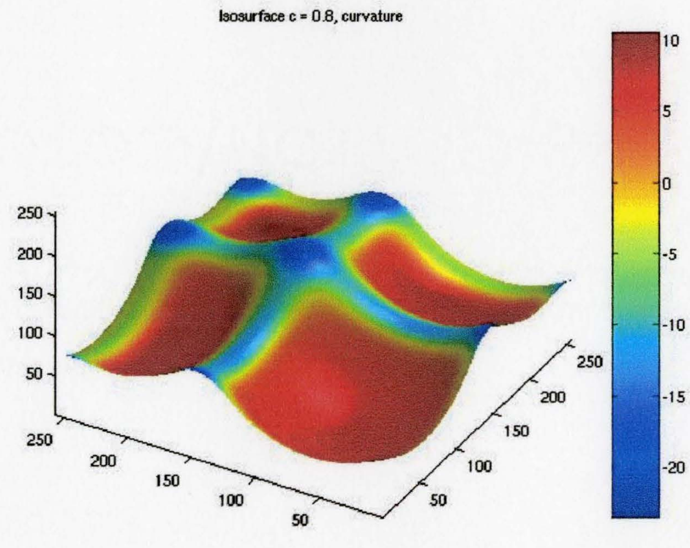


Figure 4.7: Curvature on the isosurface of $c$=0.8 at $t$=0.16. Products are located above the flame and reactants are on the bottom of the domain. The flame propagates from the top to the bottom.

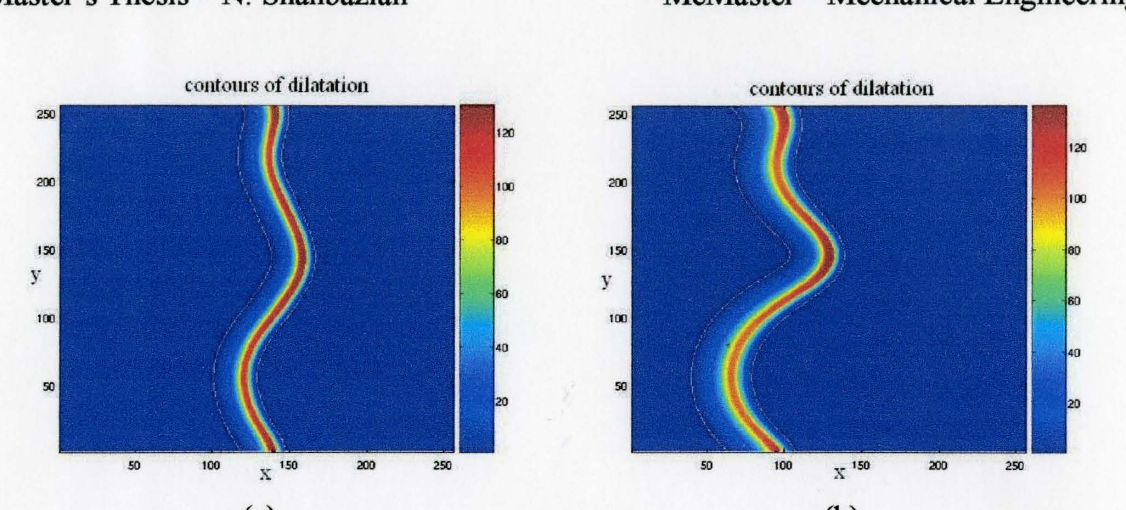


Figure 4.8: Contours of dilatation in the *x-y* plane at $z$=0.5 in two different time steps. Reactants are located on the left side of the domain while products are on the right. The three white lines indicate the progress variable isosurfaces at $c$=0.01, $c$=0.8 and $c$=0.99 (a) $t$=0.08 (b) $t$=0.16.

Figure 4.8 shows the contours of dilatation in the *x-y* plane. The cusp formation is clear from the figure. The wrinkled flame shape is influenced by the shape of initially imposed flame which is dominated by large scales. The wavelengths here are not determined by the turbulent flow and are relatively fixed. The curvature values at the bulges show a small increase with time while the negative cusp curvatures increase significantly as time progresses due to the flame propagation. Figure 4.8b shows that the flame brush thickens with time. If the domain was longer, Huygen's propagation would sharpen the cusps further, and then eventually flatten the flame. This effect is seen in appendix A for laminar two-dimensional sinusoidal flames. It can be noted that the highest dilatation occurs in a region around the isosurface of highest reaction rate, $c$=0.8 which is in consistent with the results for the turbulent case in part 4.1 and with Swaminathan *et al.* (1997).

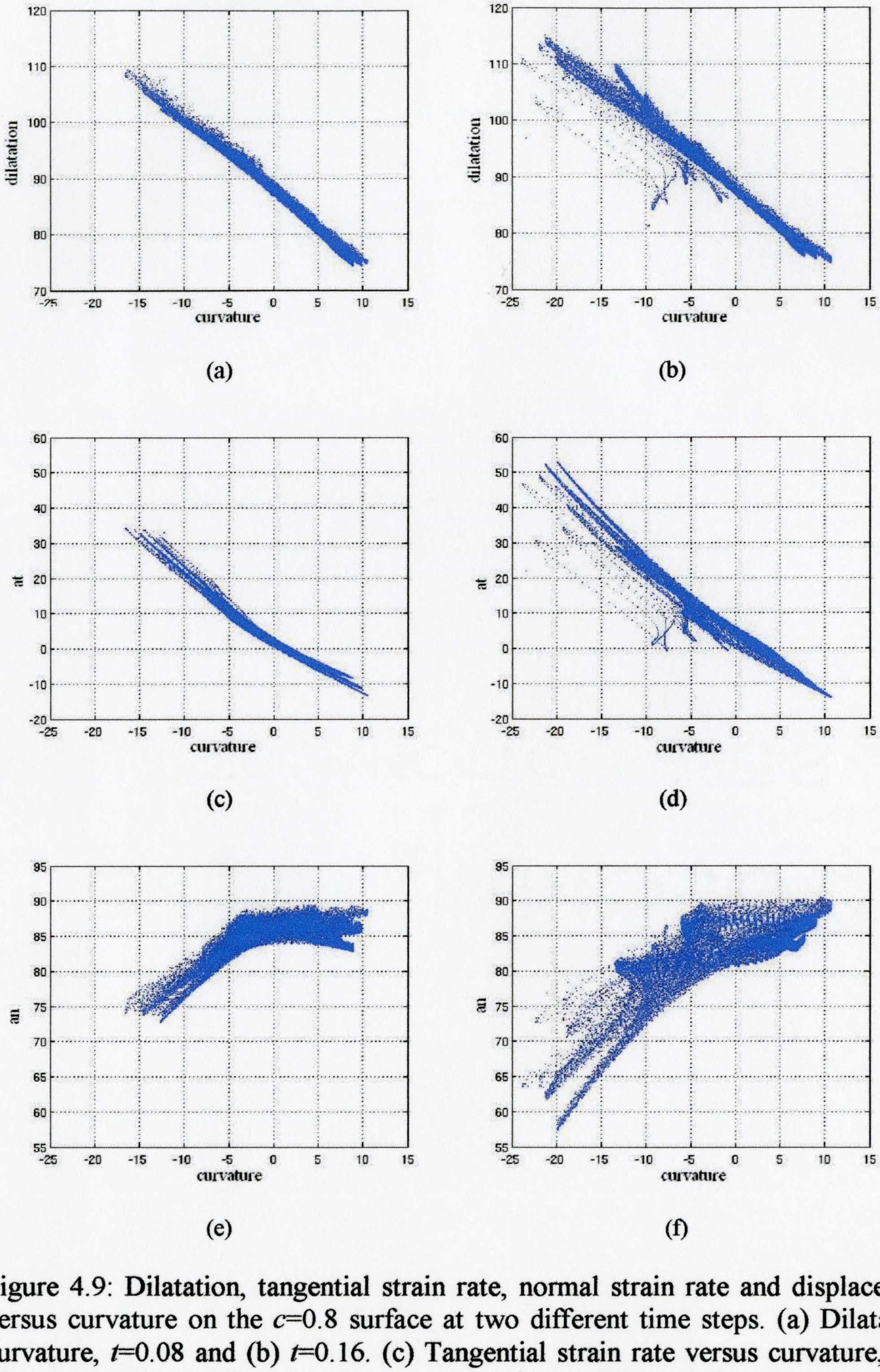


Figure 4.9: Dilatation, tangential strain rate, normal strain rate and displacement speed versus curvature on the $c$=0.8 surface at two different time steps. (a) Dilatation versus curvature, $t$=0.08 and (b) $t$=0.16. (c) Tangential strain rate versus curvature, $t$=0.08 and (d) $t$=0.16. (e) Normal strain rate versus curvature, $t$=0.08 and (f) $t$=0.16.

Plots of the dilatation and its component strains versus curvature for $t$=0.08 and $t$=0.16 are shown in figure 4.9. The same patterns are seen as in the turbulent wrinkled flame; a very linear relationship between dilatation and curvature. The effect of time seems to be small in these figures. However, as time progresses, scatter increases. There is a negative correlation between tangential strain rate and curvature as it is seen in figures 4.9c and 4.9d. These results contradicts Haworth and Poinsot (1992) and Chakraborty and Cant's (2004) analysis for the correlation between tangential strain rate and curvature. According to them, this correlation is a result of asymmetry of turbulence in two sides of the flame. Here, the reactant flow is laminar and the same correlation is observed. The negative correlation between tangential strain rate and curvature is then solely a result of heat release. Divergence of the flow streamlines on the negative curvature regions cause an expansive (positive) tangential strain rate at cusps. On the other hand, the convergence of the flow on bulges makes a compressive tangential strain rate.

At high negative curvatures (cusps) the flame tangential and normal strains deflect from the linear behaviour seen by the dilatation. For more tightly curved cusps (relative to the flame thickness), this deflection increases. This is seen for both the laminar and fully turbulent cases, where the cusps sharpen with increasing time due to propagation. It can then be concluded that the slightly nonlinear behavior of $a_t$ and $a_n$ curves is due to curvature and cusp formation rather than turbulence effects.

The plots in figure 4.9 appear to be composed of three main overlapping sets of data, particularly at higher negative curvatures. This is due to the asymmetry of the flame wrinkling which can be seen in figure 4.7. Differences between the surroundings of cusps peaks make each cusp behave slightly differently despite of having the same curvature value.

### *4.3 Turbulent $\tau$=0 Flame*

To observe the effect of turbulence on a propagating surface, a case with zero heat release ($\tau$=0) is considered. Two back to back flames are inserted into a turbulent flow field. The flames still propagate in the turbulent field due to reaction-diffusion, but without heat release and its subsequent density change and dilatation, they do not have any effect on the flow field.

The curvature on the two back to back isosurfaces of $c$=0.8 are shown in figure 4.10. The figure shows that the flames are wrinkled by turbulent eddies, and that large regions of positive curvature (bulges) are separated by narrow ridges of negative curvature (cusps). This is due to Huygen's propagation which occurs for surfaces propagating normal to themselves and is not dependent on heat release.

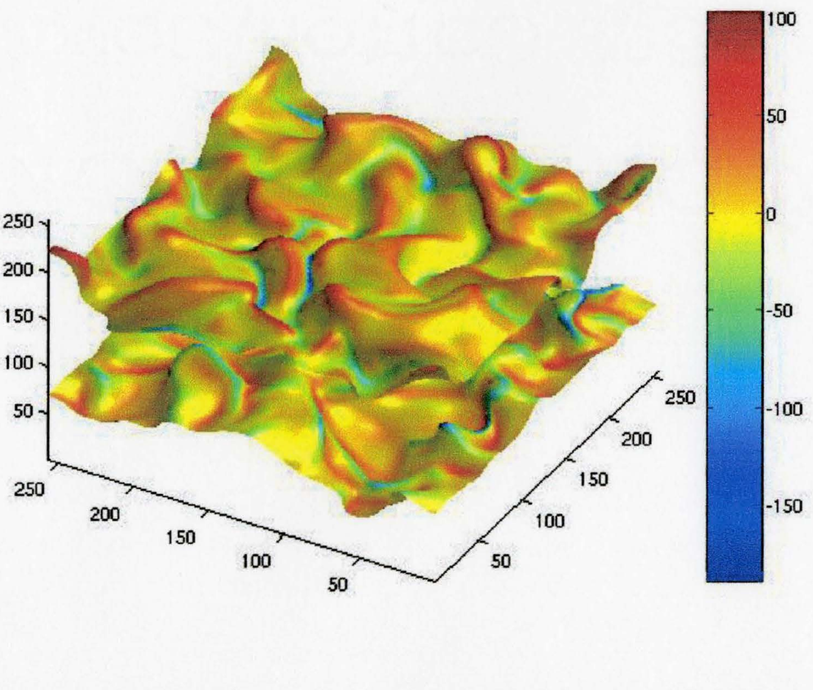


Figure 4.10: Isosurfaces of $c$=0.8 for the two back to back turbulent $\tau$=0 flames, at $t$=0.08. The surfaces are coloured by flame curvature. Products are located between two flames and reactants are at the top and at the bottom of the domain.

A material surface in a turbulent field is convected to regions of higher positive tangential strains. Both positive and negative curvature regions then align with positive strains, although the relationship between strain and curvature is not constant (Girimaji and Pope, 1992). If the surface is propagating, the alignment and the average tangential strain rate is decreased as the flame has a limited time to be transported by the turbulence, further complicating the strain-curvature relationship.

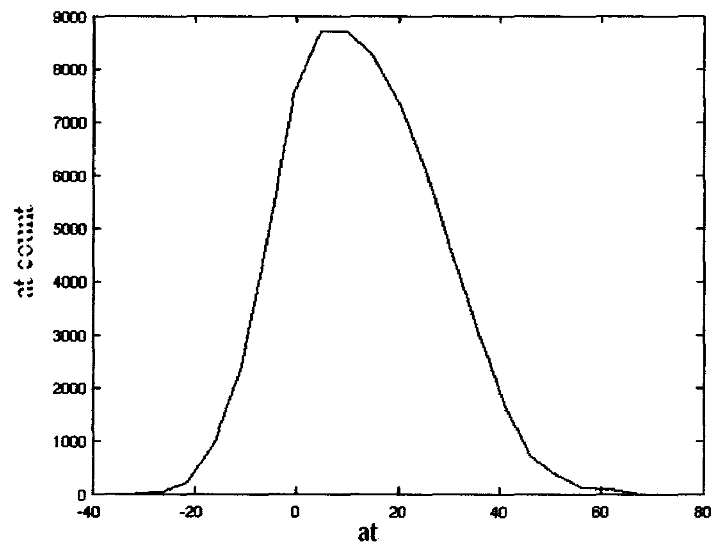


Figure 4.11: PDF of tangential strain rate at $t$=0.08.

Since dilatation in this case is zero due to absence of heat release, $a_t = -a_n$. Therefore, we only need to discuss one of the strains. PDF of tangential strain rate is shown in figure 4.11. It can be seen that there is a large skew towards positive tangential strains. This is due to the alignment of the flame surface with most expansive strains.

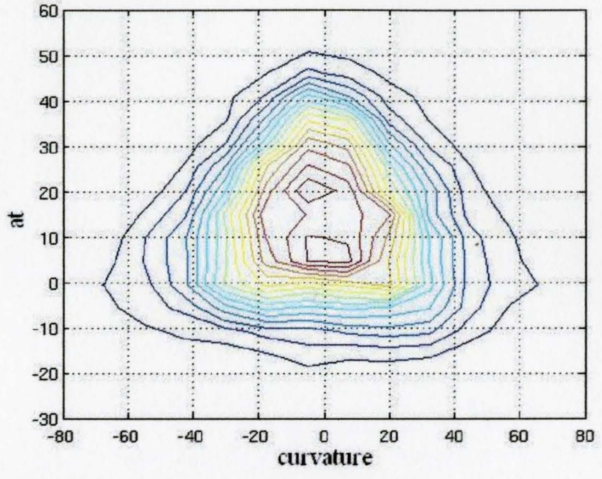


Figure 4.12: Contours of joint PDF of tangential strain rate and curvature on the $c$=0.8 surface at $t$=0.08.

The joint PDF of tangential strain rate and curvature for $t$=0.08 is shown in figure 4.12. No strong correlation is seen between tangential strain rate and curvature. A similar result was seen by Cant (1999). The highest tangential strain rate is experienced by essentially flat (zero curvature) surfaces. Girimaji and Pope (1992) explained this behaviour as the strain acting to flatten the flame, so that here, zero curvatures are the effect rather than cause of high tangential strain rates, although this does not preclude zero curvatures in regions of low tangential strain. It can be seen that tangential strain rate in figure 4.12 has large scatter at zero curvature regions. The increased scatter in the flame tangential (and normal) strains seen in the fully turbulent case with heat release (Figure 4.5) is then most likely due to the same reasons as when $\tau$=0, turbulence and the tendency of the flame to align itself with the most expansive strains.

### *4.4 Combination of Results from Sections 4.2 and 4.3*

Two separate cases have been run to isolate the effect of heat release and turbulence on the flame. The results of a laminar wrinkled flame with heat release were explained in section 4.2 and section 4.3 presented the turbulent flame with no heat release. By combining the results from laminar sinusoidal flame (Figure 4.9) and turbulent flame with no heat release (Figure 4.12), we can explain the flame behaviour in turbulent premixed flame with heat release presented in section 4.1 (Figure 4.5). The scatter seen for zero curvature in joint PDFs of tangential and normal strain rates versus curvature in turbulence case with heat release (Figure 4.5) is due to turbulence effects since the same scatter is seen in figure 4.12. This is superimposed on the negative correlation between tangential strain rate and curvature and slightly curved shape of joint PDFs in very negative curvature regions (Figure 4.5c and 4.5d) due to dilatation and heat release and not the turbulence. The same correlation was seen in figure 4.9 for the laminar sinusoidal flame.

### *4.5 Laminar Sinusoidal Flame with a Different Reaction Rate Profile*

To explore the effect of peak location in reaction rate profile, the sinusoidal laminar flame described in part 4.2 was repeated with a different reaction rate profile. Changes in correlation between dilatation and curvature from changing peak reaction area and the effect of focusing of reactants and heat in front of the flame are investigated. In this case, the peak in the reaction rate is located towards the reactant side of the flame at approximately $c$=0.32. This type of reaction rate profile is similar to hydrogen flames, as opposed to the original profile that is more typical of hydrocarbon flames. For convenience, these two profiles will be referred to as $H_2$ and $CH_4$ flames in this section.

Figure 4.13 depicts contours of dilatation in the *x-y* plane and in the middle of the domain for the two different time steps. As time progresses, the flame thickens dramatically due to the low reaction rate at the product side of the flame. Here, the completion of final reaction is slow while the advection speed of products is high which results in flame thickening.

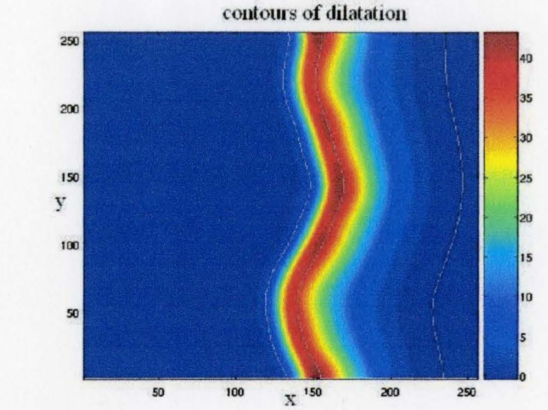


(a)

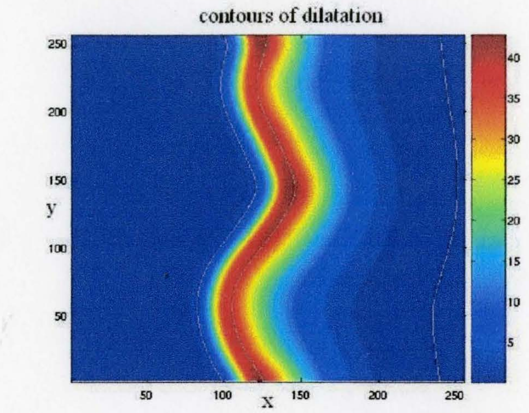


(b)

Figure 4.13: Contours of dilatation in the *x-y* plane at $z$=0.5. The three white contour lines indicate the progress variable isosurfaces at $c$=0.01, $c$=0.32 and $c$=0.99. Products are on the right side of the flame and reactants are located on the left. (a) $t$=0.04 (b) $t$=0.08.

Figure 4.13 shows that the locations of peak of dilatation and reaction rate coincide as in the original $CH_4$ flame reaction rate profile. This $H_2$ flame also shows the development of sharp cusps, although to a less extent due to the increased flame thickness.

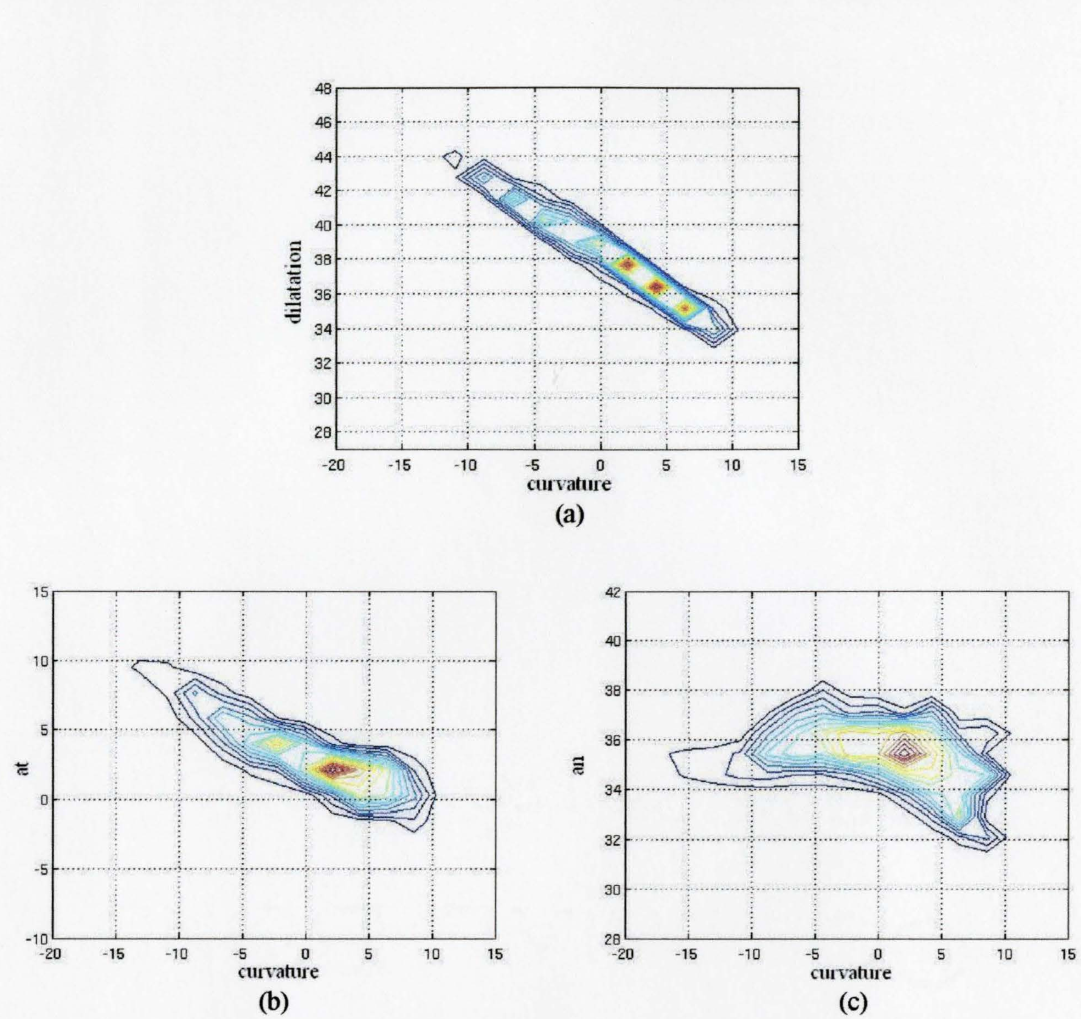


Figure 4.14: Contours of joint PDFs of dilatation, tangential strain rate, normal strain rate and curvature on the $c$=0.32 isosurface at $t$=0.08. (a) Joint PDF of dilatation and curvature. (b) Joint PDF of tangential strain rate and curvature. (c) Joint PDF of normal strain rate and curvature.

Contours of dilatation, tangential and normal strain rates versus curvature on the $c$=0.32 isosurface and $t$=0.08 are shown in figure 4.14. The negative correlation between dilatation and curvature is same as the original reaction rate profile case. The magnitude of dilatation at zero curvature is approximately 2.3 times less than $CH_4$ flame. The slope of the correlation is also reduced by about 2.3. This is mainly due to the increased flame thickness reducing the $c$ gradients. That the location of peak reaction rate does not change the dilatation-curvature correlation suggests that focusing of heat and reactants in front of the flame is the main mechanism, not simply the total area of the peak reaction rate region changing with curvature. The joint PDF of tangential strain rate versus curvature shows same negative correlation as $CH_4$ flames (including the kink in curve where slope of negative curvatures is greater than slope for positive curvatures), with a reduction in magnitude by approximately two. Very little negative $a_t$ seen on the flame. Normal strain rate is essentially uniform ($a_n$~35) regardless of curvature. Perhaps it is slightly reduced for maximum positive curvatures, unlike $CH_4$ flames where $a_n$ reduced for negative curvature.

In conclusion, the behaviour of dilatation, $a_t$ and $a_n$ versus curvature is same whether the peak reaction rate is toward the front (reactant side) or back (product side) of the flame. This is somewhat expected as these are still considered thin flames and will always be thin with respect to their curvatures. The actual values of dilatation, $a_t$ and $a_n$ are though, of course, influenced by the flame thickness ($|\nabla c|$).

# Chapter 5

# Conclusions and Recommendations for Future Work

The objective of this investigation was to gain a better understanding of the interrelationship between dilatation, tangential and normal strains and displacement speed in turbulent premixed flames. This was done by using three-dimensional compressible direct numerical simulations of turbulent and laminar premixed flames using one-step Arrhenius chemistry. One-step chemistry can be used since the flames are located in the corrugated and wrinkled flamelet regimes and the validity of this assumption shown. A main case of a fully turbulent flame was carried out and the results analyzed at two time steps, corresponding to different $u'$ and $l_t$ levels. To isolate the effect of turbulence and flame heat release, two additional cases have been run: a case with the same turbulent properties as the original case but with zero heat release ($\tau$=0), and a sinusoidally wrinkled flame with heat release in a laminar flow. To compare the effect of reaction rate profile and its peak on the flame dilatation and strain, a similar simulation on the sinusoidal laminar flame was performed using a different reaction rate profile where the peak reaction rate is closer to reactant side of the flame.

## *5.1 Conclusions*

For a turbulent premixed flame, a strong linear correlation between dilatation and flame curvature is seen over the full range of curvatures experienced. Dilatation is related to flame displacement speed and $|\nabla c|$. For these thin wrinkled flames, $|\nabla c|$ varies little with curvature and it is almost constant. The linear correlation between dilatation and curvature is then mainly due to a similar dependence of the flame displacement speed on the curvature; however, at the cusps (where the curvature is essentially the same size as the flame thickness) this direct relationship does not totally hold. The flame thickness increases right at the cusps, with an overall effect on the dilatation that retains its linear behaviour.

A similar effect is also seen in the flame tangential strain; a linear dependence on curvature but with a breakdown associated with the curvature reaching the scale of the flame thickness at the cusps. The linear correlation between tangential strain rate and curvature was explained to be due mainly to the dilatation and not the turbulence. Dilatation across a positively (negatively) curved flame surface produces negative or compressive (positive or expansive) values of $a_t$. There is a slight shift to the flame aligning most with positive tangential strain rates and a scatter is seen on tangential strain rate at zero curvatures presumably due to turbulence as this was seen in the case with no heat release. The flame normal strain is just the difference between the essentially linear dilatation and the tangential strain rate. The normal strain rate does not have a strong correlation with curvature. However like $a_t$, shows a scatter mostly on zero curvatures due to the turbulence.

For an initially sinusoidally wrinkled flame in a laminar flow, the similar results were seen for dilatation, displacement speed and strains correlations with curvature. The flame forms cusps and the cusps get sharper by time. Very linear negative correlation between dilatation and curvature were observed. This linear relationship is due to the similar linear correlation between displacement speed and curvature combined with an almost constant flame thickness ($|\nabla c|$). A negative correlation between tangential strain rate and curvature has been seen. This negative correlation in a laminar wrinkled flame contradicts some previous hypotheses on the $a_t$-curvature relationship in turbulent flames. Chakraborty and Cant (2004) and Haworth and Poinsot (1992) explained this correlation based on the different levels of turbulence in front and behind the flame. However, in the present case the wrinkled flame is not turbulent and still the same correlation can be seen. The correlation between $a_t$ and curvature is not as linear as the dilatation correlation with curvature. The tangential strain rate increases at cusps, and as the flame propagates further and the cusps get sharper, this nonlinearity increases.

For the cold turbulent flame with zero heat release, both positively and negatively curved regions of the flame aligned mostly with positive tangential strain rates. There was not an obvious correlation between $a_t$ and curvature in this case. The zero curvature regions seemed to have the highest tangential strain rate and the scatter was maximum in these points. It was reasoned that the scatter in the joint PDFs of $a_t$ and $a_n$ with curvature for the turbulent heat releasing case was due to turbulence and strain alignment as it was similar to that seen in the $\tau$=0 case.

By changing the peak reaction location of laminar sinusoidal flame towards the reactants side of the flame, the flame thickens due to the low reaction rate at the product side of the flame. The trends for correlations between dilatation, tangential and normal strain rates with curvature on the peak reaction rate isosurface are similar to the sinusoidal laminar flame with an original peak reaction rate location. However, since the flame was thicker in this case, the amounts of dilatation, tangential and normal strain rates decreased.

### *5.2 Recommendations for Future Work*

A number of DNS studies have been done on turbulent premixed flames with the correlations between different flame properties plotted. However, little work has focused on understanding the displacement speed correlation with curvature and its subsequent relationship to dilatation. The dependency of these correlations on Lewis number and effects of heat and diffusion focusing at the cusps could also be studied.

Future work would include a broader range of turbulent velocities especially relative to the heat release (so a larger range of $N_B = u'/\tau S_L$). In order to alleviate the outlet boundary problems larger $u'/S_L$ values would introduce, a turbulence damping mesh at the outlet boundaries (Wasistho, 1997) could be used. More complex chemistry including two-step or even the classic four-step methane mechanisms could also be considered. Unless one is considering flames approaching or in the thin reaction zone regime, the use of more detailed chemistry is probably unwarranted.

LES subgrid scale (SGS) models for the filtered reaction rate and the SGS scalar fluxes often include terms for the velocity gradient which is related to $a_n$. A model for $a_n$ would then be based on the dilatation and $a_t$. In an LES context, the model for the dilatation would be based directly on its curvature dependence or on its relationship with $S_d$. The model for the subgrid scale $a_t$ would include the two contributions found in this thesis: a turbulent portion that could be related to the resolved tangential strain rate and a portion due to the dilatation and SGS curvature.

# References


Abdel-Gayed, R.G., D. Bradley, M.N. Hamid and M. Lawes, Lewis Number Effects on Turbulent Burning Velocity, *Proceedings of the Combustion Institute* 20:505-512, 1984.

Ashurst, W.T., Vortex Simulation of Unsteady Wrinkled Laminar Flames, *Combustion Science and Technology* 52:325-351, 1987

Ashurst, W. T. and P.K. Barr, Stochastic Calculation of Laminar Wrinkled Flame Propagation via Vortex Dynamics, *Combustion Science and Technology* 34:227-256, 1983.

Ashurst, W.T., A.R. Kerstein, R.M. Kerr and C.H. Gibson, Alignment of vorticity and scalar gradient with strain rate in simulated Navier-Stokes turbulence, *Physics of Fluids* 30:2342-2353, 1987.

Ashurst, W.T. and I.G. Shepherd, Flame Front Curvature Distributions in a Turbulent Premixed Flame Zone, *Combustion Science and Technology* 124:115-144, 1997.

Batchelor, G.K. and A.A. Townsend, Decay of Turbulence in the Final Period, Proceedings of the Royal Society of London. Series A, Mathematical and Physical Sciences 194:527-543, 1948.

Baum, M., T.J. Poinsot and D.C. Haworth, Using Direct Numerical Simulations to study H2/O2/N2 flames with complex chemistry in turbulent flows, *9th Symposium on Turbulent Shear Flows*, Kyoto, Japan, 25-2-1, 25-2-6, 1993.

Baum, M., T. Poinsot, D. Haworth and N. Darabiha, Direct numerical simulation of H2/02/N2 flames with complex chemistry in two-dimensional turbulent flows, *Journal of Fluid Mechanics* 281:1-32, 1994.

Bell, J.B., R.K. Cheng, M.S. Day and I.G. Shepherd, Numerical simulation of Lewis number effects on lean premixed turbulent flames, *Proceedings of the Combustion Institute* 31:1309–1317, 2007.

Bell, J.B, M.S. Day and J.F Grcar, Numerical Simulation of Premixed Turbulent Methane Combustion, *Proceedings of the Combustion Institute* 29:1987-1993, 2002.

Bennett, J.C. and S. Corrsin, Small Reynolds number nearly isotropic turbulence in a straight duct and a contraction, *Physics of Fluids* 21:2129-2140, 1978.

Borghi, R., On the Structure of Turbulent Premixed Flames, *Recent Advance in Aeronautical Science*, Editors: C. Bruno and C. Casc, Pergamon, 1984.

Bradley, D., P.H. Gaskell, A. Sedaghat and X.J. Gu, Generation of PDFS for flame curvature and for flame stretch rate in premixed turbulent combustion. Combustion and Flame 135:503-523, 2003.

Cant, R.S., Direct Numerical Simulation of Premixed Turbulent Flames, *Philosophical Transaction, The Royal Society London A* 357:3583-3604, 1999.

Cant, R.S., C. Rutland and A. Trouve, Statistics for laminar flamelet modelling, In Proceedings of the Summer Program, Center for Turbulence Research, Stanford University/NASA-Ames, pp. 271-279, 1990.

Chakraborty, N., Comparison of displacement speed statistics of turbulent premixed flames in the regimes representing combustion in corrugated flamelets and thin reaction zones, *Physics of Fluids* 19:105109, 2007.

Chakraborty, N. and R.S. Cant, Tangential strain rate and curvature effects on displacement speed of an unsteady turbulent premixed flame in a quasi-steady configuration, *1st European Combustion Meeting*, Orleans, France, 2003

Chakraborty, N. and S. Cant, Unsteady effects of strain rate and curvature on turbulent premixed flames in an inflow–outflow configuration, Combustion and Flame 137:129-147, 2004.

Chakraborty, N. and R.S. Cant, Effects of strain rate and curvature on surface density function transport in turbulent premixed flames in the thin reaction zones regime, *Physics of Fluids* 17:065108, 2005a.

Chakraborty, N. and R.S. Cant, Influence of Lewis number on curvature effects in turbulent premixed flame propagation in the thin reaction zones regime, *Physics of Fluids* 17:105105, 2005b.

Chakraborty, N. and R.S. Cant, Influence of Lewis number on strain rate effects in turbulent premixed flame propagation, *International Journal of Heat and Mass Transfer* 49:2158-2172, 2006.

Chakraborty, N., E.R. Hawkes, J.H. Chen and R.S. Cant, The effects of strain rate and curvature on surface density function transport in turbulent premixed methane–air and hydrogen–air flames: A comparative study, *Combustion and Flame* 154:259-280, 2008.

Chakraborty, N., M. Klein and R.S. Cant, Stretch rate effects on displacement speed in turbulent premixed flame kernels in the thin reaction zones regime, *Proceedings of the Combustion Institute* 31:1385–1392, 2007.

Chakraborty, N. and N. Swaminathan, Influence of the Damköhler number on turbulence-scalar interaction in premixed flames. II. Model development, *Physics of Fluids* 19:045104, 2007.

Chen, J.H., T. Echekki and W. Kollmann, The Mechanism of Two-Dimensional Pocket Formation in Lean Premixed Methane-Air Flames with Implications to Turbulent Combustion, *Combustion and Flame* 116:15-48, 1999.

Chen, J.H. and H.G. Im, Correlation of Flame Speed with Stretch in Turbulent Premixed Methane/Air Flames, *Proceedings of the Combustion Institute* 27:819-826, 1998.

Courant, R., K. Friedrichs and H. Lewy, On the Partial Difference Equations of Mathematical Physics, Mathematische Annalen 100:32-74, 1928.

Damköhler, G., The Effect of Turbulent on the Flame Velocity in Gas Mixtures, *Z. Elektrchem* 46:601-652, 1940 (English translation NACA Tech. Mem. 1112, 1947).

Dandekar, A. and L. Collins, Effect of Nonunity Lewis Number on Premixed Flame Propagation through Isotropic Turbulence, *Combustion and Flame* 101:428-440, 1995.

Davidson, L., *Numerical Methods for Turbulent Flows*, http://www.tfd.chalmers.se/gr-kurs/MTF071, Chalmers University of technology, Sweden, 2005.

Davidson, P.A., Turbulence: An Introduction for Scientists and Engineers. 1st ed. Oxford University Press, 2004.

Echekki, T. and J.H. Chen, Unsteady Strain Rate and Curvature Effects in Turbulent Premixed Methane-Air Flames, *Combustion and Flame* 106:184-202, 1996.

Echekki, T. and J.H. Chen, Analysis of the contribution of curvature to premixed flame propagation, *Combustion and Flame* 118:308-311, 1999.

El Tahry, S.H., C. Rutland and J. Ferziger, Structure and Propagation Speeds of Turbulent Premixed Flames- A Numerical Study, *Combustion and Flame* 83:155-173, 1993.

George, W.K., *Lectures in Turbulence for the 21st century*, Chalmers University of Technology, Gothenburg, Sweden, 2002.

Girimaji, S.S. and S.B. Pope, Propagating surfaces in isotropic turbulence, *Journal of Fluid Mechanics* 234:247-277, 1992.

Gülder, Ö.L, Turbulent premixed flame propagation models for different combustion regimes, 23rd Symposium (International) on Combustion 23:743-750, 1991.

Hawkes, E.R. and J.H. Chen, Direct numerical simulation of hydrogen-enriched lean premixed methane–air flames, *Combustion and Flame* 138:242-258, 2004.

Hawkes, E.R. and J.H. Chen, Comparison of direct numerical simulation of lean premixed methane–air flames with strained laminar flame calculations, *Combustion and Flame* 144:112–125, 2006.

Haworth, D.C. and T.J. Poinsot, Numerical simulations of Lewis number effects in turbulent premixed flames, *Journal of Fluid Mechanics* 244:405-436, 1992.

Jenkins K.W and R.S. Cant, Direct numerical simulation of turbulent flame kernels, *Recent Advances in DNS and LES*, Editors: D. Kinght and L. Sakell, New York: Kluwer Academic Publishers, pp. 191–202, 1999.

Jenkins K.W and R.S. Cant, Flame Kernel Interactions in a Turbulent Environment, *In DNS/LES Progress and Challenges*, Editors: C. Liu and L. Sakell and T. Beutner, Columbus, OH: Greyden Press, 2001.

Jenkins, K.W., M. Klein, N. Chakraborty and R.S. Cant, Effects of strain rate and curvature on the propagation of a spherical flame kernel in the thin-reaction-zones regime, *Combustion and Flame* 145:415-434, 2006.

Jime´nez, C., B. Cuenot, T. Poinsot and D. Haworth, Numerical Simulation and Modeling for Lean Stratified Propane-Air Flames, *Combustion and Flame* 128:1–21, 2002.

Kolmogorov, A.N., The local structure of turbulence in incompressible viscous fluid for very large Reynolds numbers, *Dokl. Akad. Nauk SSSR* 30:301-305, 1941.

Kostiuk, L.W. and K.N.C. Bray, Mean Effects of Stretch on Laminar Flamelets in a Premixed Turbulent Flame, *Combustion Science and Technology* 95:193-212, 1992.

Laverdant, A.M. and S.M. Candel, Computation of Diffusion and Premixed Flames Rolled Up in Vortex Structures, *Journal of Propulsion and Power* 5:134-143, 1989.

Law, C.K. and C.J. Sung, Structure, aerodynamics, and geometry of premixed flamelets, *Progress in Energy and Combustion Science* 26:459–505, 2000.

Mayo, J.R. and A.R. Kerstein, Scaling of Huygens-front speedup in weakly random media, *Physics Letters A* 372:5–11, 2007.

Nada, Y., M. Tanahashi and T. Miyauchi, Effect of turbulence characteristics on local flame structure of H2–air premixed flames, *Journal of Turbulence* 5:1-15, 2004.

Nye, D.A., T.W. Lee and D.A. Santavicca, Flame stretch measurements during the interaction of premixed flames and Kármán vortex streets using PIV, *Combustion and Flame* 105:167-179, 1996.

Orszag, S.A. and G.S. Patterson, Numerical Simulation of Three-Dimensional Homogeneous Isotropic Turbulence, *Physical Review Letters* 28:76-79, 1972.

Patnaik, G. and K. Kzailasanath, Cellular structure of lean hydrogen flames in microgravity, *28th AIAA Aerospace Sciences Meeting*, Reno, AIAA Paper 90-0041, 1990.

Peters, N., The turbulent burning velocity for large-scale and small-scale turbulence, *Journal of Fluid Mechanics* 384:107-132, 1999.

Peters, N., P. Terhoeven, J.H. Chen and T. Echekki, Statistics of Flame Displacement Speeds from Computations of 2-D Unsteady Methane-Air Flames, *Proceedings of the Combustion Institute* 27:833-839, 1998.

Poinsot, T., S. Candel and A. Trouve, Applications of direct numerical simulation to premixed turbulent combustion, *Progress in Energy and Combustion Science* 21:531-576, 1996.

Poinsot, Echekki and Mungal, A study of the laminar flame tip and implications for premixed turbulent combustion, Combustion Science and Technology 81:45-73, 1992

Poinsot, T. and S.K. Lele, Boundary Conditions for Direct Simulations of Compressible Viscous Flows, *Journal of Computational Physics* 101:104-129, 1992.

Poinsot T. and D. Veynante, *Theoretical and numerical combustion*. 2nd ed. Philadelphia: R.T. Edwards, 2005.

Poinsot, T., D. Veynante and S. Candel, Quenching processes and premixed turbulent combustion diagrams, *Journal of Fluid Mechanics* 228:561-605, 1991.

Pope, S.B., *Turbulent Flows*. 1st ed. Cambridge: Cambridge University Press, 2000.

Renou, B., A. Boukhalfa, D. Peuchberty and M. Trinite, Effects of Stretch on the Local Structure of Freely Propagating Premixed Low-Turbulence Flames with Various Lewis Numbers, *Proceedings of the Combustion Institute* 27:841-847, 1998.

Rogallo, R.S., Numerical Experiments in Homogeneous Turbulence, NASA TM 81315, NASA Ames Research Center, CA, 1981.

Rutland, C.J. and S. Cant, Turbulent transport in premixed flames, *In Proceedings of the Summer Program*, Center for Turbulence Research, Stanford University./NASA-Ames, pp 75-94, 1994.

Rutland, C. J. and J. Ferziger, Interaction of a vortex structure and a premixed flame, *27th AIAA Aerospace Sciences Meeting*, Reno, AIAA Report 89-0127, 1989.

Rutland, C. J. and A. Trouve, Premixed flame simulations for non-unity Lewis number, In Proceedings of the Summer Program, Center for Turbulence Research. NASA Ames/Stanford University, pp. 299-310, 1990.

Rutland, C.J. and A Trouve, Direct simulations of premixed turbulent flames with nonunity Lewis numbers, *Combustion and Flame* 94:41-57, 1993.

Schumann, U. and G.S. Patterson, Numerical study of the return of axisymmetric turbulence to isotropy, *Journal of Fluid Mechanics* 88:711-735, 1978.

Sung, C.J., C.J. Sun and C.K. Law, Analytic description of the evolution of two-dimensional flame surfaces, *Combustion and Flame* 107:114-124, 1996.

Swaminathan, N., R.W. Bilger and B. Cuenot, Relationship Between Turbulent Scalar Flux and Conditional Dilatation in Premixed Flames with Complex Chemistry, *Combustion and Flame* 126:1764-1779, 2001.

Swaminathan, N., R.W. Bilger and G.R. Ruetsch, Interdependence of the instantaneous flame front structure and the overall scalar flux in turbulent premixed flames , *Combustion Science and Technology* 128:73-97, 1997.

Tavoularis, S., J.C. Bennett and S. Corrsin, Velocity-derivative skewness in small Reynolds number, nearly isotropic turbulence, Journal of Fluid Mechanics 88:63-69, 1978.

The´venin, D., Three-dimensional direct simulations and structure of expanding turbulent methane flames, *Proceedings of the Combustion Institute* 30:629–637, 2005.

Trouve, A. and T. Poinsot, The evolution equation for the flame surface density in turbulent premixed combustion, *Journal of Fluid Mechanics* 278:1-31, 1994.

Tullis, S. and R.S. Cant, Scalar transport modeling in large eddy simulation of turbulent premixed flames, *Proceedings of the Combustion Institute* 29:2097-2104, 2002.

Wasistho, B., B.J. Geurts and J.G.M. Kuerten, Simulations techniques for spatially evolving instabilities in compressible flow over a flat plate, *Computers and Fluids* 26: 713, 1997.

Wray, A.A., *Minimal Storage Time Advancement Schemes for Spectral Methods*, unpublished report, NASA Ames Research Center, 1990.

Yeung, P. K., S.S. Girimaji and S.B. Pope, Straining and Scalar Dissipation on Material Surfaces in Turbulence: Implications for Flamelets, *Combustion and Flame* 79:340-365, 1990.

Zhang, S. and C. Rutland, Premixed Flame Effects on Turbulence and Pressure-Related Terms, *Combustion and Flame* 102:447-461, 1995.

# Appendix A

# Preliminary Analysis

Before running the main simulations, some validations on the boundary conditions, initial conditions and turbulence properties have been performed.

## *A.1 Testing the Differentiators*

In order to test the differentiators, the following velocity profiles were set as differentiators input:

$$U = \sin\left(\frac{2\pi}{128}(ic-1)\right) \tag{A.1}$$

$$V = \sin\left(\frac{2\pi}{128}(jc-1)\right) \tag{A.2}$$

$$W = \sin\left(\frac{2\pi}{128}(kc-1)\right) \tag{A.3}$$

where *U*, *V* and *W* are velocities in *x*, *y* and *z* directions respectively and *ic*, *jc* and *kc* represent the nodes in each direction in $128^3$ grid.

The output of differentiators for $\frac{dU}{dx}$ and $\frac{d^2U}{dx^2}$ were plotted versus *x*. The plot matched the analytical expression for the differentiators. The output was smooth for periodic and outflow boundaries. In the case of periodic boundary condition, the results wrapped around on the boundaries. The same observations apply to differential operators when used on *V* and *W* velocities.

For testing the cross differentiators, for example $\frac{d^2U}{dxy}$, the $U$ velocity is defined as follows:

$$U = \sin\left(\frac{2\pi}{128}(ic-1)\right) * \sin\left(\frac{4\pi}{128}(jc-1)\right) \tag{A.4}$$

The validation procedure is same as before.

### *A.2 Testing the Initial Energy Function Spectra*

From a large number of identical experiments, the velocity ensemble average can be given by: (George, 2002)

$$\langle u_i(\vec{x},t)\rangle = \overline{u}_i(\vec{x},t) \equiv \lim_{N\to\infty}\frac{1}{N}\sum_{n=1}^{N} u_i^{(n)}(\vec{x},t) \tag{A.5}$$

For the homogenous turbulence, the two point correlation is defined as: (Pope, 2000)

$$R_{ij}(\vec{r},t) \equiv \langle u_i(\vec{x}+\vec{r},t)u_j(\vec{x},t)\rangle \tag{A.6}$$

which is independent of $\vec{x}$.

The one-dimensional spectra $E_{ij}(\kappa_1)$ are defined to be twice the one-dimensional Fourier transform of $R_{ij}(\vec{e}_1 r_1)$ where $\vec{e}_1$ is the unit vector in the $x_1$-coordinate direction (Pope, 2000).

$$E_{ij}(\kappa_1) \equiv \frac{1}{\pi}\int_{-\infty}^{+\infty} R_{ij}(\vec{e}_1 r_1)e^{-i\kappa_1 r_1}dr_1 \tag{A.7}$$

$\vec{\kappa} = \{\kappa_1, \kappa_2, \kappa_3\}$ is the wavenumber vector and $|\vec{\kappa}| = \kappa = \frac{2\pi}{l}$ where $l$ is the wave-length.

So $\kappa_1 = e_1 \cdot \vec{\kappa}$

For isotropic turbulence, the three-dimensional energy function spectrum can be calculated as: (Pope, 2000)

$$E(\kappa) = \frac{1}{2}\kappa^3 \frac{d}{d\kappa}\left(\frac{1}{\kappa}\frac{dE_{11}(\kappa)}{d\kappa}\right) \tag{A.8}$$

In a turbulent flow, kinetic energy is extracted from the mean flow by the large eddies. This energy is then transferred by smaller eddied to the smaller ones. At the smallest scales, the kinetic energy is transferred into internal energy which is called dissipation. The scale of the smallest eddies is determined by viscosity and increase of internal energy or dissipation (Davidson, 2005). The length scale of the smallest eddies is called the Kolmogorov length scale (Kolmogorov, 1941).

Reynolds number for the energy containing eddied is defined as following while $l_t$ is the integral length scale and $u'$ is the fluctuating velocity of turbulent flow.

$$\mathrm{Re}_t = \frac{u' l_t}{\nu} \tag{A.9}$$

The spectral method of Rogallo (1981) was tested. We compared the specified initial energy spectrum with the initial velocity field calculated by DNS. Then the one-dimensional energy function spectrum was calculated from both the initial velocity correlations and the specified three-dimensional energy spectrum. The energy spectra compared quite well. So the initial velocity field generated from the specified three-dimensional energy spectrum was acceptable.

For the cold turbulent case, the one-dimensional and three-dimensional initial energy spectra are plotted in figure A.1. The calculations were performed for a case of $256^3$ with:

$\kappa_{\min} = 1 \times 2\pi$, $\kappa_{peak} = 4 \times 2\pi$, $\kappa_{\max} = 128 \times 2\pi$ and $\gamma_E = 1.41 \times 10^{-3}$

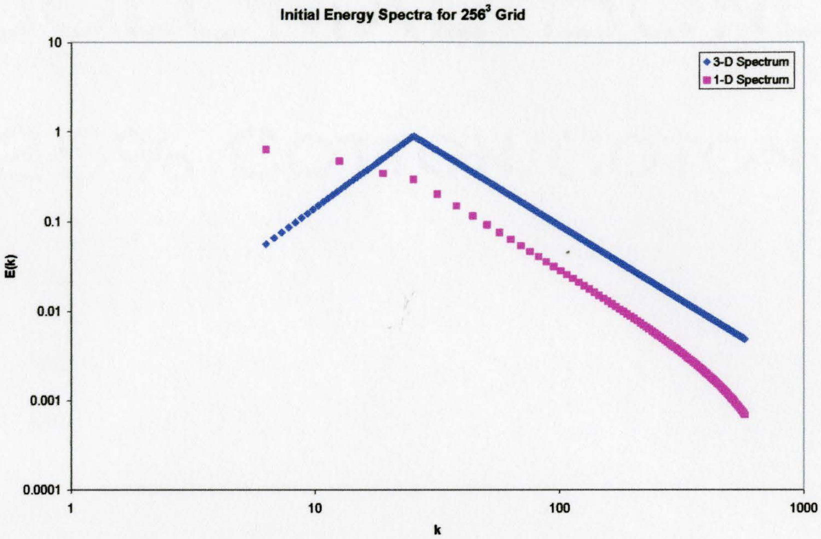


Figure A.1: Initial one-dimensional and three-dimensional energy spectra.

To test the isotropy of the initial velocity field, the one-dimensional energy spectra as defined in equation A.7 were calculated from nine different velocity correlations.

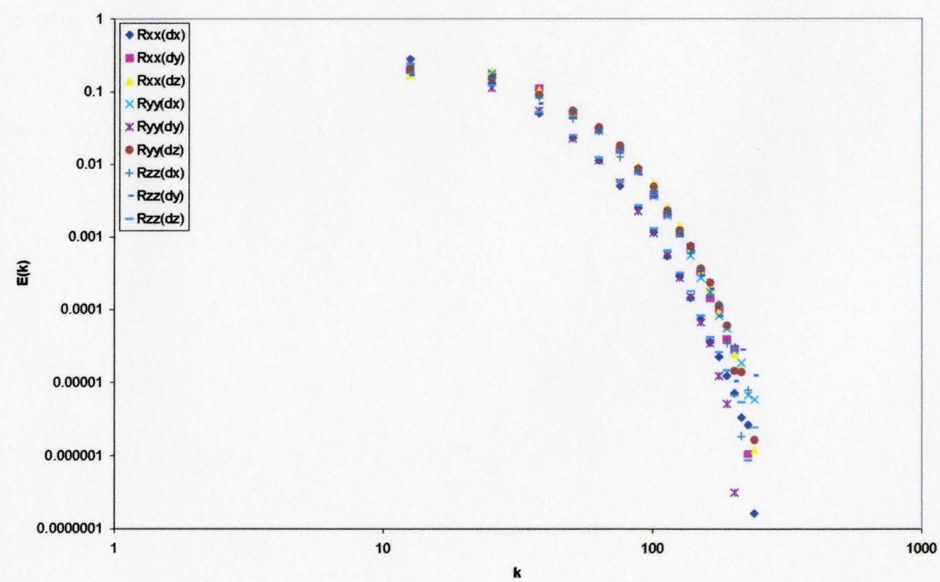


Figure A.2: One-dimensional energy spectra.

From figure A.2, it is observed that all six transverse correlations coincide as well as all three longitudinal correlations. As a result, the velocity field is isotropic.

### *A.3 Skewness*

The skewness factor of the velocity derivatives $\frac{\partial u_i}{\partial x_i}$ is a measurement for energy transport by inertial terms from low to high wavenumbers (Schumann and Patterson, 1978) (Bennett and Corrsin, 1978) and for isotropic turbulence it is defined as:

$$S_{u_i} = -\frac{\overline{\left({\partial u_i}/{\partial x_i}\right)^3}}{\left[\overline{\left({\partial u_i}/{\partial x_i}\right)^2}\right]^{3/2}} \tag{A.10}$$

When the skewness of velocity derivative reaches a constant value, turbulence can be considered as developed or free of unphysical characteristics of the initial conditions (Tavoularis *et al.*, 1978). Figure A.3 shows the time development of the velocity derivative in x direction for the turbulent flow in $256^3$ grid previously mentioned. The value of skewness stays relatively constant on slightly below 0.5 after $t$=0.006.

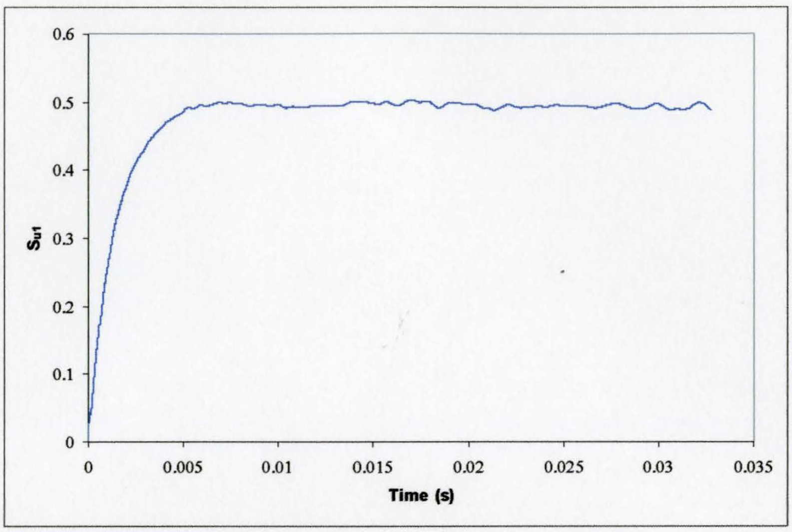


Figure A.3: Time development of skewness of velocity derivative in the $x$ direction.

### *A.4 Grid Independency*

As mentioned earlier, turbulent flow wrinkles the flame and as a result, flame may get thinner locally. To ensure that the thinner parts of flame are resolvable by the grid and the result is grid independent, a planar laminar flame is simulated in both $128^3$ and $256^3$ grids. The progress variable along the box is shown in figure A.4 for these two grids at different time steps. The similar results are observed for two different grids which indicate the grid independence of the simulations.

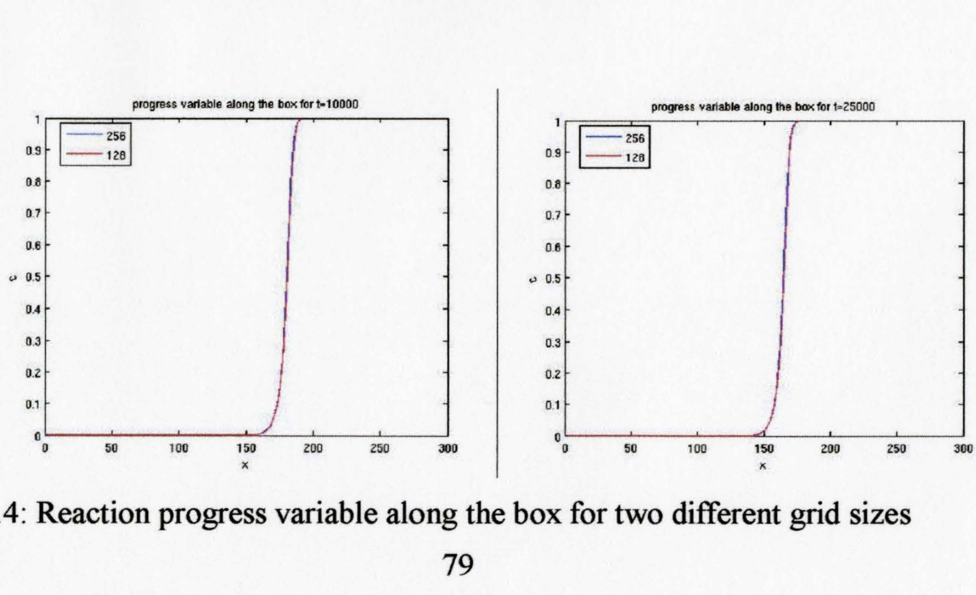


Figure A.4: Reaction progress variable along the box for two different grid sizes

For the 128 grid, there are 7 grid points in the flame thickness while for 256 grid, there are 14 points.

# Appendix B

# Two-dimensional Laminar Back to Back Flames

The purpose of this simulation is to consider the long term evolution of a wrinkled laminar flame. Two back to back flames are inserted in a laminar flow field (the flow velocity is initially set to zero). The flames are sinusoidal in the $y$ direction with amplitude of 0.04 and wavenumber of 2. The size of the box in this case is extended to 10 in $x$-direction and remained 1 for two other directions. The number of grid points of $768\times128\times12$ is used for this simulation which indicates that the domain is only resolved in two dimensions. By adjusting $B^*$, Prandtl and Schmidt numbers, a laminar flame speed $S_L$=1.16 and a flame thickness of 0.089 are obtained. The number of grid points in the $x$-direction is set in order to have about 7 grid points inside the flame. The parameters used for this simulation are shown in table B.1.

| | |
|---|---|
| Heat release factor, $\tau$ | 3 |
| $\alpha=\tau/(1+\tau)$ | 0.75 |
| Zeldovich number, $\beta$ | 8 |
| Pre-exponential factor, $B^*$ | 2450 |
| Ratio of specific heats, $\gamma$ | 1.4 |
| Reynolds number, $Re=1/\nu$ | 25 |
| Mach number, $Ma$ | 0.014159 |
| Prandtl number, $Pr$ | 0.7 |
| Schmidt number, $Sc$ | 0.7 |
| Lewis number, $Le$ | 1 |
| Grid spacing, $\Delta x$ | 0.013 |
| Grid spacing, $\Delta y$ | 0.0078 |
| Time step, $\Delta t$ | $5\times10^{-6}$ |
| Laminar flame speed, $S_L$ | 1.16 |
| Laminar flame thickness, $\delta_L$ | 0.089 |

Table B.1: Parameters used for the laminar sinusoidal flame case.

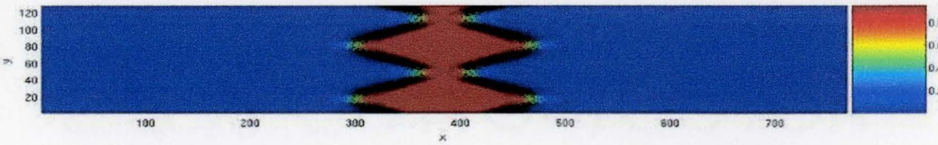


*t=0*

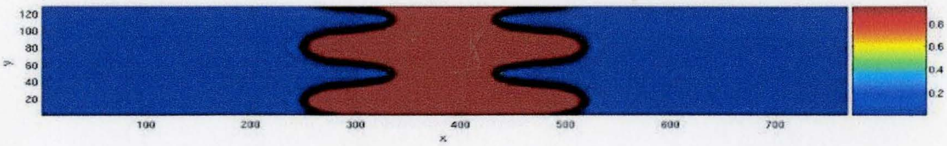


*t=0.05*

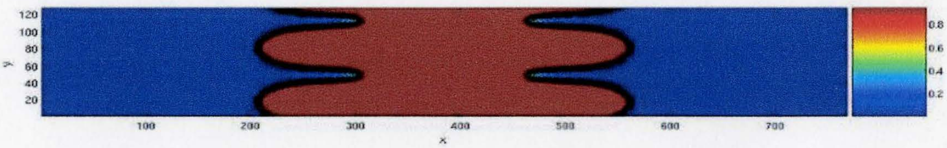


*t=0.1*

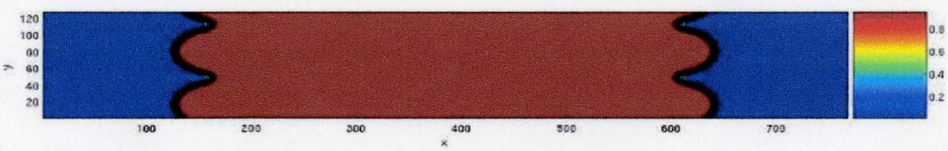


*t=0.2*


*t=0.3*

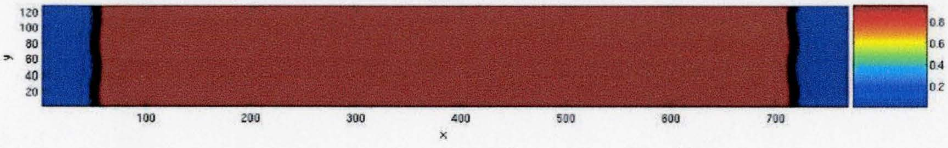


*t=0.4*

*t=0.475*

Figure B.1: Contours of progress variable in *x-y* plane at $z$=0.5 for the laminar sinusoidal flame in different time steps.

As it is clear from the figures, cusps are formed when the flames propagate towards the reactants. The cusp formation is mainly due to the flame front propagation normal to itself with a constant velocity relative to the flow field (Huygen's propagation). Since the box is longer in the *x*-direction (and $\tau$=3) compared to the other cases in this study, the flames have a longer time to evolve before they reach the edge of the domain. It can be seen that after developing cusps, the initially wrinkled flames flatten with time until they exit the domain while almost planar. This is also a feature of Huygen's propagation. For negative curvature regions, the effect of curvature makes the cusps move faster as seen from the figure B.2. So the flame speed enhances while the positive curvature regions tend to the planar laminar flame speed (Law and Sung, 2000). Therefore, an initially wrinkled flame flattens out with time (Mayo and Kerstein, 2007). This effect can only be seen in this case study due to the high length of the box in the flame propagation direction.

Figure B.2: Smoothing effects of curvature on wrinkled flames (Law and Sung, 2000).